THESIS FOR THE DEGREE OF DOCTOR OF PHILOSOPHY

Energy Harvesting for Wireless and Less-Wired Sensors in Gas Turbines

ELOF KÖHLER

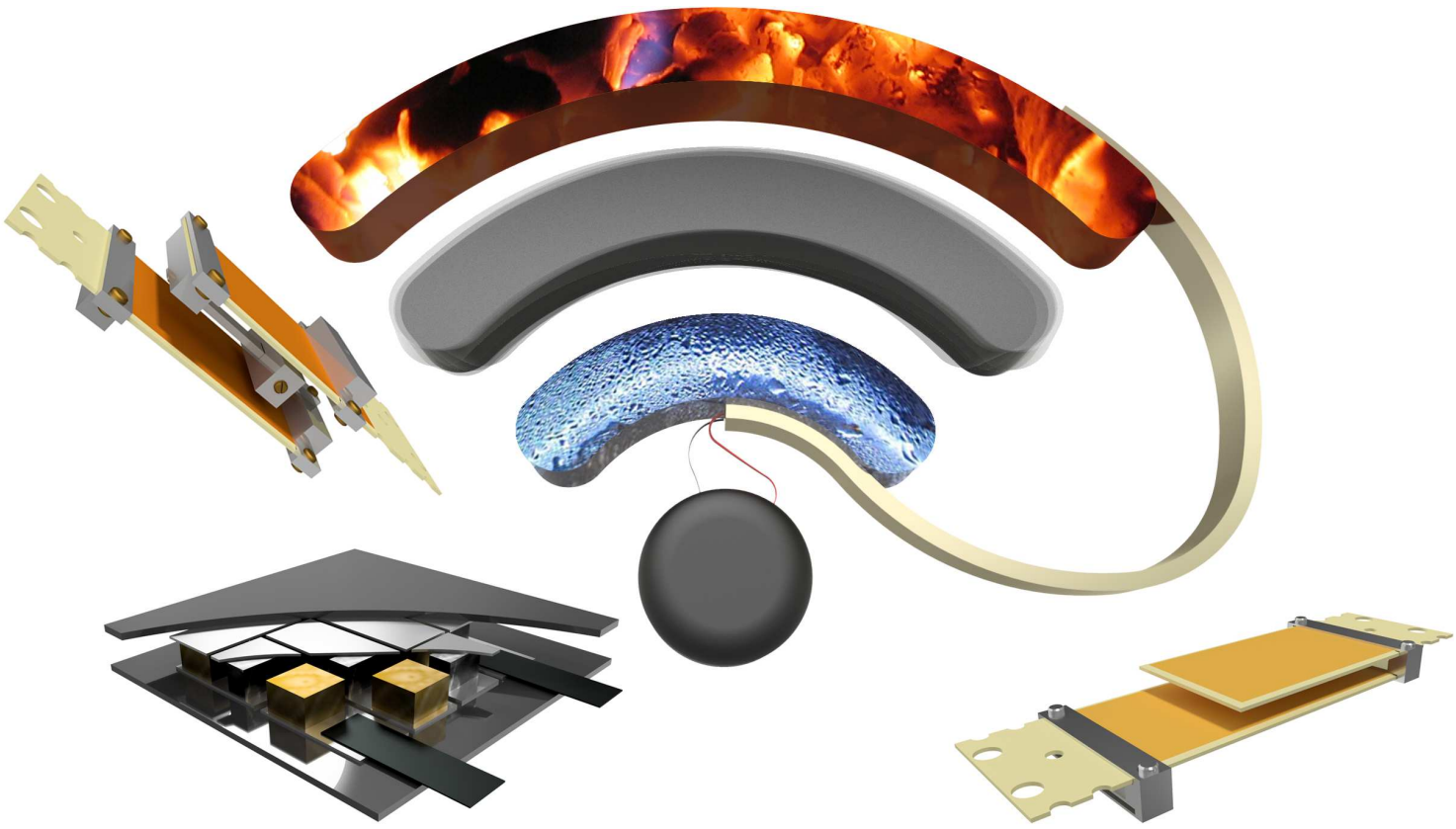

Department of Microtechnology and Nanoscience
CHALMERS UNIVERSITY OF TECHNOLOGY
Göteborg, Sweden, 2019

Energy Harvesting for Wireless and Less-Wired Sensors in Gas Turbines
ELOF KÖHLER
ISBN 978-91-7905-131-0

Doktorsavhandlingar vid Chalmers Tekniska Högskola
Ny serie nr. 4598
ISSN 0346-718X

Technical report MC2-415
ISSN 1652-0769

Micro and Nanosystems Group
Electronic Materials and Systems Laboratory
Department of Microtechnology and Nanoscience
Chalmers University of Technology
SE–412 96 Gothenburg
Sweden
Telephone +46 (0)31–772 1000

Printed by Chalmers Reproservice
Göteborg, Sweden, 2019

Det finns inga dåliga kläder, bara dåliga väder.

Energy Harvesting for Wireless and Less-Wired Sensors in Gas Turbines
ELOF KÖHLER
Department of Microtechnology and Nanoscience
Chalmers University of Technology

Abstract

Four types of energy harvesters aimed for gas turbine applications were developed during this thesis. The unique gas turbine environment shaped the design- and material choices. A semiconductor thermoelectric harvester was built for a location in the gas turbine with active cooling at 600°C, with 800°C wall temperature. The thesis covers the material synthesis, design, assembly and proof-of-concept tests of this harvester at 800°C. A metal thermoelectric harvester was also built, but instead for locations without active cooling. The harvester design is long metal strips, capable of reaching active cooling far away. This harvester was successfully used to power wireless sensors and reached 290 μW power output after power management electronics. Two different types of piezoelectric harvesters were developed, both consisting of coupled off-the-shelf cantilevers. The development included simulations, analytic models and assembly/measurements on harvesters. The first design was a 2-degree-of-freedom folded coupled harvester which after optimizations achieved a minimum of 2.75 V in the frequency range $92-162$ Hz with peak power output of 1.80 mW. The second design was a 4-degree-of-freedom self-tuning harvester, showing increased 3 dB-bandwidth from 8 Hz to 12 Hz with the use of a sliding weight.

Keywords: Energy harvester, harsh environment, thermoelectric, piezoelectric, thermoelectric harvester, piezoelectric harvester, coupled harvester, self-tuning

Acknowledgments

I would like to thank the following people:

My deep gratitude to my supervisor and examiner Peter Enoksson for all the support, guidance, discussions and inspiration.

My co-supervisor Anders Palmqvist for your support and knowledge and my co-supervisor Torbjörn Nilsson for the excellent proofreading.

Henrik Staaf for the scientific collaborations, the discussions about everything and the fun during both travel and work.

Richard Heijl for all your help with the thermoelectric materials.

Per Lundgren for making teaching something I enjoy and want to improve in.

Sofia, Volodomyr, Mazharul, Amin, Agin, Anderson, Markus and Qi for the scientific collaborations and the nice atmosphere at work.

Sanel Zenkic, Anders Lindblom and Edvard Svenman at GKN Aerospace, James Roberts at Rolls Royce PLC®, Dhasarathy Parthasarathy at Volvo Technology, John Kemp and Michael Allen at Coventry University, Marios Christodoulou at SCITEK consultants LTD and Cristina Rusu at Rise Acreo for nice collaborations and help with measurements.

My dad for proofreading this thesis.

Patric and Mattias for all the awesome coffee breaks.

Elof Köhler
Gothenburg, Sweden
May, 2019

List of Publications

Paper I

High Temperature Energy Harvester for Wireless Sensors
E. Köhler, R. Heijl, L.G.H. Staaf, S. Zenkic, E. Svenman, A. Lindblom, A. Palmqvist and P. Enoksson
In *Smart Materials and Structures*,
Vol. 23, 095042, 2014.

Paper II

Analytic Modeling of a High Temperature Thermoelectric Module for Wireless Sensors
E. Köhler, L.G.H Staaf, A. Palmqvist and P. Enoksson
In *Journal of Physics: Conference Series 557*,
Vol. 557, 012085, 2014

Paper III

Metal Thermoelectric Harvester for Wireless Sensors
E. Köhler, T.M.J. Nilsson and P. Enoksson
Submitted

Paper IV

Simulation and Experimental Demonstration of Improved Efficiency in Coupled Piezoelectric Cantilevers by Extended Strain Distribution
L.G.H. Staaf, E. Köhler, D. Parthasarathy, P. Lundgren and P. Enoksson
In *Sensors and Actuators A: Physical*,
Vol. 229, p. 136-140, 2015

Paper V

Impact of Designed Asymmetries on the Effective Bandwidth of a Backfolded Piezoelectric Energy Harvester
E. Köhler, L.G.H. Staaf, A. Smith, P.D. Folkow, P. Lundgren and P. Enoksson
In *Sensors and Actuators, A: Physical*,
Vol 292, p 77-89, 2019

Paper VI

Achieving Increased Bandwidth for 4 Degrees of Freedom Self-Tuning Energy Harvester
L.G.H. Staaf, A. D. Smith, E. Köhler, P. Lundgren, P. Folkow and P. Enoksson
In *Journal of Sound and Vibration*,
Vol. 420, p. 165-173, 2018

Contributions

Paper I

Responsible for design, analytic modeling, assembly, measurements on module and partly synthesis. Author of manuscript, synthesis exluded.

Paper II

Responsible for all parts.

Paper III

Responsible for all parts.

Paper IV

Partly responsible for building device, simulation strategies, measurement setup and measurements. Partly responsible for ideas and partly responsible for writing conclusion.

Paper V

Partly responsible for building device, simulation strategies, measurement setup and measurements. Partly responsible for ideas. Main author of manuscript.

Paper VI

Partly responsible for measurement setup, measurements, writing and idea.

Other publications

— Not appended due to overlap —

Verification of self-tuning 4DOF piezoelectric energy harvester with enhanced bandwidth

L.G.H Staaf, E. Köhler, A. Smith, P. Folkow and P. Enoksson

In *The 17th international conference on Micro and Nanotechnology for Power Generation and Energy Conservation Application (PowerMEMS2017)*,
(2017)

Selftuning energy harvester by sliding weight

L.G.H Staaf, E. Köhler, P. Folkow and P. Enoksson

In *Svenska Mekanikdagarna 2017*,
(2017)

Smart design piezoelectric energy harvester with self-Tuning

L.G.H Staaf, E. Köhler, P. Folkow and P. Enoksson

In *Journal of Physics: Conference Series. 28th Micromechanics and Microsystems Europe Workshop, MME 2017*,
Vol. 922, 012007, (2017)

Piezoelectric energy harvesting as energy source for autonomous intelligent wireless systems on gas turbines

L.G.H. Staaf, E. Köhler, J. Kemp, M. Allen, S. Zenkic, A. Lindblom, M. Christodoulou, J. Roberts, P. Lundgren and P. Enoksson

In *IET Conference Publications. EVI-GTI and PIWG Joint Conference on Gas Turbine Instrumentation*,
CP.2016.0693 (2016)

Proof of concept thermoelectric energy harvester powering wireless sensor on gas turbine

E. Köhler, L.G.H Staaf, J. Kemp, M. Allen, S. Zenkic, A. Lindblom, M. Christodoulou, J. Roberts and P. Enoksson

In *IET Conference Publications. EVI-GTI and PIWG Joint Conference on Gas Turbine Instrumentation*,
CP.2016.0831 (2016)

Smart design selftuning piezoelectric energy harvester intended for gas turbines

L.G.H. Staaf, E. Köhler, M. Soeiro, P. Lundgren and P. Enoksson

In *15th International Conference on Micro and Nanotechnology for Power Generation and Energy Conversion Applications (PowerMEMS2015)*,
Vol. 660, 012125, (2015)

Modelling and experimental verification of more efficient power harvesting by coupled piezoelectric cantilevers

L.G.H. Staaf, E. Köhler, D. Parthasarathy, P. Lundgren and P. Enoksson

In *14th International Conference on Micro and Nanotechnology for Power Generation and Energy Conversion Applications (PowerMEMS2014)*,
Vol. 557, 012098, (2014)

Fabrication of High Temperature Thermoelectric Energy Harvesters for Wireless Sensors

E. Köhler, R. Heijl, L.G.H. Staaf, S. Zenkic, E. Svenman, A. Palmqvist and P. Enoksson

In *13th International Conference on Micro and Nanotechnology for Power Generation and Energy Conversion Applications (PowerMEMS2013)*,
Vol. 476, 012036, (2013)

— Not appended due to out of scope —

Mems Meander Harvester With Tungsten Proof-Mass

E. Köhler, P. Johannisson, D. Kolev, F. Ohlsson, P Ågren, J. Liljeholm, P. Enoksson and C. Rusu

In *18th International Conference on Micro and Nanotechnology for Power Generation and Energy Conversion Applications (PowerMEMS2018)*,
(2018)

Thermal Influence on the Electrochemical behavior of a supercapacitor containing an ionic liquid electrolyte

M. Hague, Q. Li, A. D. Smith, V. Kuzmenko, E. Köhler, P. Lundgren and P. Enoksson

In *Electrochimica Acta*,
(2018)

Nanocomposite materials for miniaturized supercapacitors

Q. Li, V. Kuzmenko, M. Hague, P. Lundgren, E. Köhler, L.G.H Staaf and P. Enoksson

In *International Conference and Exhibition on Integration Issues of Miniaturized Systems 2017*,
p. 199-205. (2017)

Rapid manufacturing of OSTE polymer RF-MEMS components

S. Rahiminejad, J. Hansson, E. Köhler, W. van der Wijngaart, T. Haraldsson, S. Haasl and P. Enoksson

In *Proceedings of the IEEE International Conference on Micro Electro Mechanical Systems (MEMS)*,
p. 901-904. (2017)

Miniaturized Supercapacitors for Smart Systems

Q. Li, V. Kuzmenko, M. Hague, P. Lundgren, E. Köhler, L.G.H Staaf and P. Enoksson

In *Smart Systems Integeration 2017*,
Cork, Ireland (2017)

Supercapacitor with increased capacitance at 200°C

E. Köhler, L.G.H Staaf and P. Enoksson

In *IET conference publications, EVI-GTI and PIWG joint conference on Gas Turbine Instrumentation*,
CP693 (2016)

Direct 3D printed shadow mask on Silicon

S. Rahiminejad, E. Köhler and P. Enoksson

In *27th Micromechanics and Microsystems Europe Workshop*,
Vol. 757, 012021, (2016)

Evaluation of 3D printed materials used to print WR10 horn antennas

E. Köhler, S. Rahiminejad and P. Enoksson

In *27th Micromechanics and Microsystems Europe Workshop*,
Vol. 757, 012026, (2016)

MEMS Based Micro Aerial Vehicles

N. Joshi, E. Köhler and P. Enoksson

In *27th Micromechanics and Microsystems Europe Workshop*,
Vol. 757, 012035, (2016)

Simulation of a Novel Bridge MEMS-PZT Energy Harvester for Tire Pressure System

E. Trabaldo, E. Köhler, L.G.H Staaf, P. Enoksson and C. Rusu

In *14th International Conference on Micro and Nanotechnology for Power Generation and Energy Conversion Applications (PowerMEMS2014)*,
Vol. 557, 012041, (2014)

List of Acronyms

TEG	Thermoelectric Generator
RTG	Radioisotope Thermoelectric Generators
zT	Figure of Merit for thermoelectric material
ZT	Figure of Merit for thermoelectric device
PZT	Lead Zirconate Titanate
RMS	Root Mean Square
PTFE	Polytetrafluoroethylene
MPPT	Maximum Power Point Tracking
NASA	National Aeronautics and Space Administration
EMIM Ac	1-Ethyl-3-methylimidazolium acetate
STARGATE	Sensors Towards Advanced Monitoring and Control of Gas Turbine Engines

Contents

CHAPTER 1

Introduction

The development of low power electronics and more efficient wireless communication has led to an increase in the use of wireless sensors, both with new sensor applications but also by replacing existing wired sensors with wireless solutions. One of the key reasons for replacing a wired sensor with a wireless sensor is to reduce the amount of wires used, reducing both the cost of the wires and the time needed to install a sensor.

However, wireless sensors require a power source to function. A battery is often preferred with the combination of high energy content, low self-discharge and low cost. If for some reason the environment is not suitable for batteries (e.g. if the temperature is too high, if the sensor is inaccessible under long periods of time or the peak power is too high) the battery should be replaced or combined with other power source solutions. Also, even if the wireless sensor can be battery powered for many years it can be beneficial to combine it with an energy harvester to increase the life time further. To have, for example, a car or a truck to go into service only to change sensor batteries is impractical.

There are different levels of wireless sensing, ranging from sensors powered externally but with wireless communication [1] to neat solutions where power supply, sensor and transmitter are all combined in one package, e.g. the wireless stop bell push system for buses. Sometimes the reality is somewhere in between, and a more suitable name would then be less-wired sensors [2].

An example of possible parts involved in a wireless sensor system can be seen in Fig. 1.1, where a thermoelectric energy harvester is connected to a power management circuit. The power management circuit stores the energy inside a supercapacitor until the stored energy exceeds the requirement to start the transceiver and transmitting the sensor data.

In sensor environments where e.g. the temperature is too high for the electronics the sensors cannot be a neat wireless sensor package, instead the electronics must be on a safe distance from the sensor. It could however still be beneficial to have the energy harvester close to the sensor because of the larger energy content available in the environment.

1.1 Background and motivation

The thesis work is heavily connected to the industry and the appended papers are all a result of collaborations with various universities, gas turbine manufacturers and aerospace companies [2, 3]. The unique gas turbine environment and the high demands associated with the aerospace industry has shaped the outcome of this thesis. Various gas turbines located in test facilities in Europe has contributed to the vibrational- and temperature data used in this project and has also

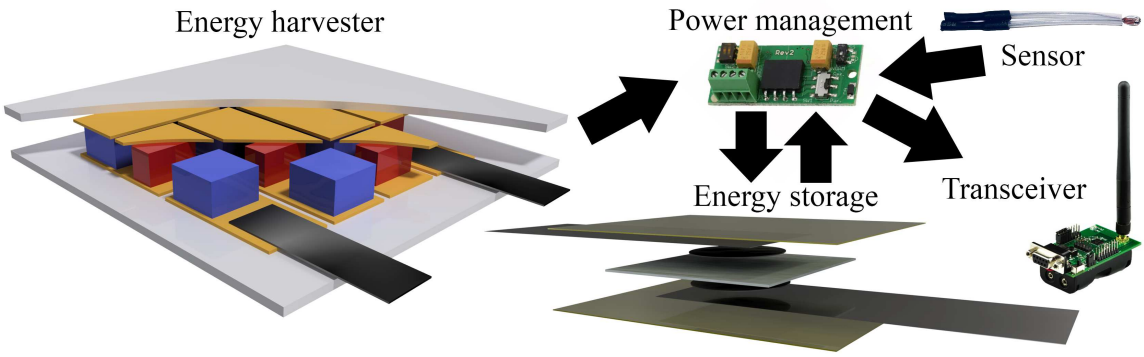

Figure 1.1: An energy harvester converts waste energy to electricity and supplies a power management circuit. The power management circuit stores energy temporarily and delivers power to the transceiver.

been subject to harvester measurements for powering wireless sensors.

The gas turbines in these test facilities can have thousands of sensors, with many of them requiring difficult wire placements. In these harsh environments the complexities of wireless sensors increase as well. However, one of the key reasons for replacing a wired sensor with a wireless or less-wired sensor is to reduce the amount of wires used, reducing both the cost of wires and the time needed to install/debug the sensor. Reduced weight can also be an additional reason for wireless sensors, e.g. in aircraft gas turbines.

Developing energy harvesters for gas turbines is a combination of energy conversion and survivability in harsh environments. It requires aerospace grade materials and cables and sometimes that electronics are placed far away from the harvester. This approach gives a different prerequisite of the harvester designs than if the harvesters are investigated without considering a specific application. Another consequence of this approach is the aim and presentation of the harvester results, with more focus on connectivity with a wireless sensor system than the more conventional power output/efficiency of the energy harvesters.

1.2 Wireless approach

Needless to say, a gas turbine has large amounts of waste energy that can be harvested (e.g. vibrations, thermal, moving parts, pressure, sound, air flow) but this also means that the electronics and the harvester needs to withstand this harsh environment. Replacing the wired sensors are all but straightforward and the harsh environment requires unique solutions to electronics and power sources for every wireless sensor. Thus, although the main topic of this thesis is energy harvesting, it is inescapable to discuss the complete wireless sensor system, because the design of the harvesters, electronics and energy storage need to be matched with the rest of the system.

With the goal to power a wireless sensor with energy harvesting, the power requirements from sensor and transmitter are important for the design. Hence, the power losses from cables, power

electronics and the self-discharge of the energy storage need to be accounted for.

1.2.1 Power source

One of the most common power sources are batteries. Batteries are easily available, inexpensive and simple to replace in easily accessed locations. However, most sensor locations in a gas turbine are not suitable for batteries, either because of high temperatures or inaccessible locations. Energy harvesters can handle higher temperatures than batteries and if coupled with energy storage such as supercapacitors they can function far longer than batteries [4].

Heat

Thermal energy is abundant in gas turbines with around 20% of the compressed air used for cooling purposes [5]. There are many methods of converting thermal energy into electrical energy, either by utilizing the temperature change (pyroelectric harvesters) [6] or the thermal gradient [7].

Most methods utilize the thermal gradient for conversion, with higher possible conversion efficiency with increasing thermal gradient [8]. Large scale mechanical conversion methods such as Rankine heat engines (steam turbines) or Brayton heat engines (gas turbines) can convert up to 40-50% of the heat energy [9]. Combined cycle power plants can reach above 60% by combining two or more methods to maximize conversion efficiency [10]. These methods are however not suitable as small-scale energy harvester solutions, with decreasing efficiency with decreasing size, eventually less efficient than thermoelectric power conversion (at approximately 10-100 W) [11].

Because thermoelectric harvesters utilize thermal gradients, they will suffer from low power output during start up, while pyroelectric harvesters would have large power output during start up and low power output at cruise speed. If power is needed during start up it is possible to combine the harvester with some energy storage [4] or combining it with a pyroelectric energy harvester.

Vibrations

It is also possible to harvest energy from sound [12] or vibrations in a gas turbine. There are several different types of energy harvester technologies to consider when building a vibrational harvester e.g. electrostatic, electromagnetic, magnetostrictive, triboelectric, piezoelectric and more [13–18]. The optimal location for a vibrational harvester in a gas turbine is where the temperature is too high for batteries, but not as high as for the thermal harvester.

Capacitive harvesters do not work well in high temperatures as high temperatures can reduce the electret stability [19]. Magnetostrictive energy harvesters have been shown to work at temperatures of at least 225°C but with some loss in power output at higher temperatures [20]. Work on high temperature piezoelectric energy harvesters has resulted in harvesters capable of

250-300°C, although these harvesters suffers from reduced power output at temperatures above 200°C [21, 22].

However, vibrational energy harvesters need to fulfil some basic conditions before coupled with a self-powering miniaturized system; namely reaching minimum voltage-/power output required for the self-powering system and to manage this within the natural frequency of the environment. This requires a good match between the harvester's natural frequency and the environment. In an environment with fluctuating natural frequency this increases the demands for a harvester design with broad bandwidth. Figure 1.2 illustrates the harvester amplification (blue area) together with the acceleration profile of the environment.

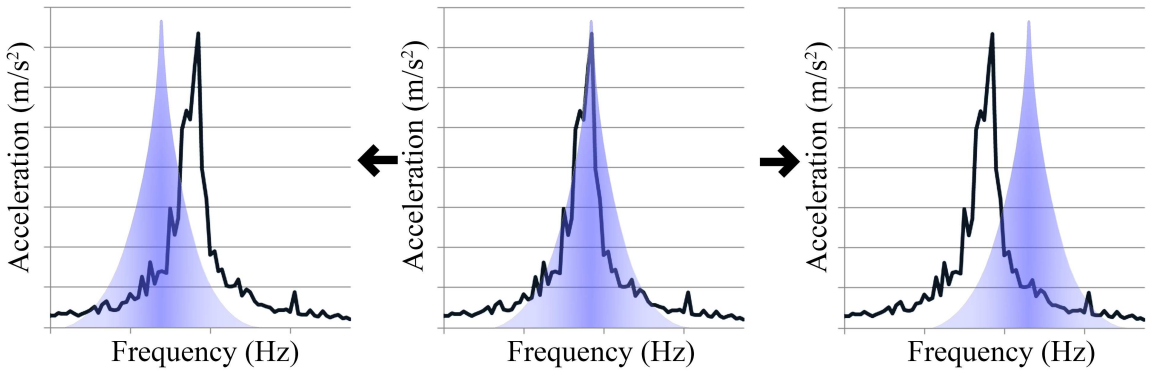

Figure 1.2: Acceleration as a function of frequency for the environment (black line) with blue shape representing the amplification from a cantilever.

There are several methods available for modifying bandwidth, power output and resonance frequency in vibrational cantilevers. One way to enhance the power output is to change a rectangular cantilever to a narrowing geometric shape (trapezoidal shape [23]), since the part closest to the attached end of a rectangular cantilever receives most of the stress distribution and therefore corresponds to the main part of the power output [24]. A tip mass can be attached on the cantilever in order to adjust and lower the eigenfrequency to match different ambient vibrations. The applied mass also increases the bandwidth slightly, although with the possible undesirable consequence of sacrificing power output [25]. A broad bandwidth harvester can be achieved by combining several cantilevers with different eigenfrequencies in an array, see Fig. 1.3. This method requires that the single cantilevers are tuned to give a frequency overlap with the other cantilevers while still maintaining enough power output in the desired frequency region, either by modifying the eigenfrequencies by tip masses or properties (e.g. length or width) of the cantilevers.

Non-linear harvesters are a promising approach to broaden the bandwidth, with unique structural designs on cantilever level [26], strong electric fields to introduce non-linearity [27] or structural design on system level with hardening structures [28] or impact-driven harvester designs [29]. The tuning of these systems to a specific environment differs in complexity, e.g. cantilever arrays can easily be tuned to any environment, however, with increasing bandwidth requirement these harvesters also need more electronics and increased volume [30]. Non-linear

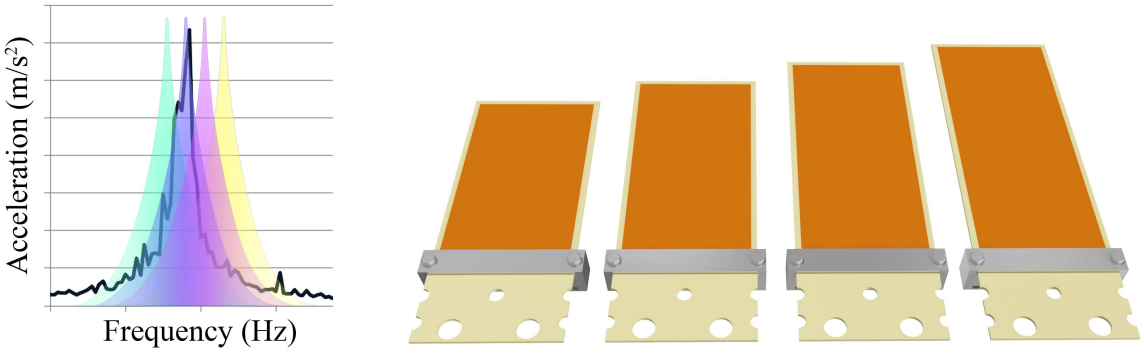

Figure 1.3: Four cantilevers with different eigenfrequencies in array.

designs with large hysteresis can be forced to jump to the more energetic of the two available stable modes with fast burst perturbation [31].

Another solution to achieve broader bandwidth is to add a second cantilever on the tip of the primary cantilever, called a 2DOF (two-degree-of-freedom) harvester, see Fig. 1.4. These harvesters tend to have more even stress distribution and they enhance the power output, compared with the combined output from two single cantilevers [24]. When tuning this type of harvester to the required resonance frequencies it can be mounted with two tip masses, one for the primary harvester and one for the secondary harvester [32–35].

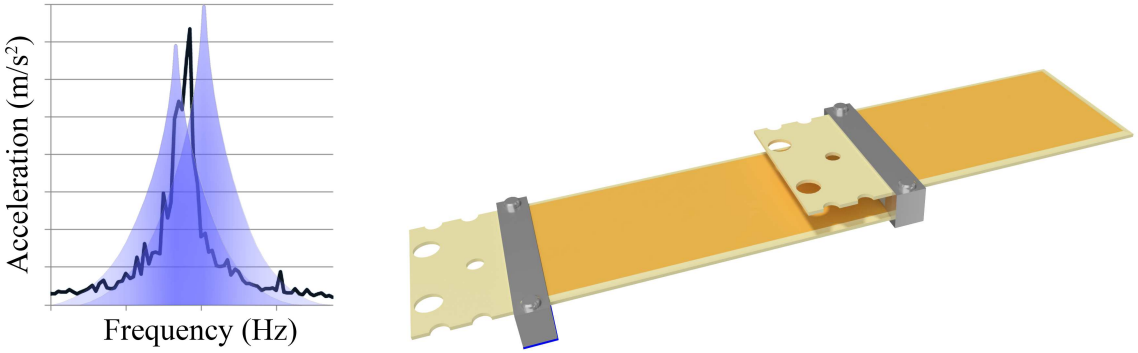

Figure 1.4: Coupled harvester with top cantilever attached at the tip of the bottom cantilever.

The first mass is applied between the primary and secondary cantilever and the second mass is applied at the tip of the secondary cantilever. This solution is more space efficient compared to an array of single cantilevers. The solution yields a broad bandwidth harvester with the power output separated into two peaks. Systems with two beams coupled in the same plane have previously been thoroughly investigated [33, 36–40].

Another concept that enables a broader bandwidth for an energy harvester is to use a self-tuning resonator. Self-tuning is when the resonance frequency of the harvester changes to better match the resonance frequency of the environment. Several ways of resonance tuning can be achieved

during operation of the harvester, both with electronics [41, 42] or mechanical solutions [43].

Self-tuning with electronics can quickly adjust the resonance frequency to increase the power output. In environments with rapid fluctuations in the resonance frequency this method can increase the power output substantially [41]. However, the electronic self-tuning requires power and should only be used if the gain is larger than the power requirement of the self-tuning electronics.

Mechanical self-tuning is achieved by altering the length [44], stiffness [45] or mass [46] of the cantilever to change the resonance frequency. Boudaoud et al. demonstrated a free to slide mass on a vibrating metal string, actuated by an oscillating magnetic field, which can self-adjust the system to certain input frequencies [47]. The free sliding mass adds one degree of freedom to the system. A different approach uses a bead inside a hollow cylindrical cantilever [48]. A more recent study from Miller et al. also achieved a self-tuning harvester behavior through a fixed-fixed beam and a sliding mass configuration [46, 49].

This thesis is limited to thermal- and vibrational methods only, specifically thermoelectric harvesters and piezoelectric harvesters. Worth noting, vibrations and noise are unwanted effects in a gas turbine and has been actively fought in the aerospace industry, with reduced average noise levels in turbofan engines by 10 dB over 30 years [50].

1.2.2 Power management

Power management have several purposes, e.g. to store energy, to convert the voltage to a suitable level and to wait until enough voltage- or power output is achieved before releasing the energy to the wireless sensor electronics to avoid stalling of the wireless electronics.

The DC-DC step up voltage boost in the power management circuit for e.g. thermoelectric harvesters can be substantial, requiring DC-DC boost from a few millivolts to several volts. DC-DC conversion solutions from 10-100 mV [51–54] to 3.3 V suffers from low efficiency (less than 50%).

Piezoelectric harvesters typically have higher voltage output than thermoelectric harvesters but instead the power management circuit has to convert AC current into DC [55]. Like the power management circuits for thermoelectric harvesters, the power management system needs to wait until enough energy is stored before attempting to power the wireless sensor node. Additional features in more advanced power management circuits for piezoelectric harvesters is maximum power point tracking (MPPT) [56] and this can improve the conversion efficiency substantially.

1.2.3 Energy storage

The start-up sequence in the wireless sensor electronics requires the most energy, reaching several mJ (8-200 mJ) and mW (10 mW or more) depending on electronics [57, 58]. In most cases the energy harvester cannot reach these power levels, thus requiring energy storage.

Supercapacitors can provide higher power outputs than batteries and be charged/discharged with very little degradation but suffers from higher self-discharge and lower energy content

than batteries [59]. Using a supercapacitor alone is not recommended because of the high self-discharge and low energy density, but a supercapacitor coupled to an energy harvester can be a powerful combination [4].

The combination of an energy harvester and a supercapacitor is extra powerful in harsh environments where e.g. heat, vibrations or high pressure are plentiful. A supercapacitor can be designed to handle vibrations and high pressures and can even get an energy density boost from operating at high temperatures [60].

1.3 Thermoelectric harvesters

Most off-the-shelf available thermoelectric generators have a maximum operating temperature below 325°C [61] with a few generators operating at higher temperatures up to 800°C [62]. At temperatures above 800°C there are no off-the-shelf generators available and to keep high efficiency several thermoelectric materials in segments are needed, making the generators much more complex [63]. These are mainly used in RTGs (radioisotope thermoelectric generators) in NASAs space missions or remote lighthouses [64, 65].

Off-the-shelf thermoelectric harvesters are stiff and flat to maximize the thermal input and output. In some situations, it is more appropriate with flexible harvesters, e.g. in wearable harvester designs [66] or to achieve good thermal contact with non-flat surfaces [67]. Harvesters with long flexible thermoelectric couples can also be used to increase the separation of the cold side and hot side [68, 69], either to decrease the thermal conductance or to reach a heat source/active cooling. The drawback of these long harvesters is the high resistance of the harvester that can reach hundreds of Ohms.

In the middle and rear part of a gas turbine the temperature can reach far above 800°C and cooling air is pumped through the walls and turbine blades to decrease the surface temperature. A thermoelectric energy harvester inside a gas turbine can be placed in one of these cooling channels. In the middle of a gas turbine the sensor cables are the longest and most difficult to place. Replacing these with wireless sensors or less wired sensors is highly desirable.

The harvester in the cooling channel (**paper I** and **paper II**) is not designed to be purely efficient, instead it is designed to take advantage of the excessive heat to give a good power/mass ratio (W/kg). The size was decided to be 12 mm$\times$12 mm$\times$3 mm and the materials were chosen to be $Ba_8Ga_{16}Ge_{30}$ and La-doped $Yb_{14}MnSb_{11}$. These materials have their peak efficiency in this temperature span and can operate at up to 800°C.

Locations on the gas turbine without direct active cooling is also interesting for wireless sensing. Unfortunately, thermoelectric harvesters are not suitable for areas with low thermal gradients. A solution to increase the length of a thermoelectric harvester to reach active cooling is proposed in (**paper III**), with all-metal thermoelectric couples and good load resistance matching with the power management electronics, see Fig. 1.5.

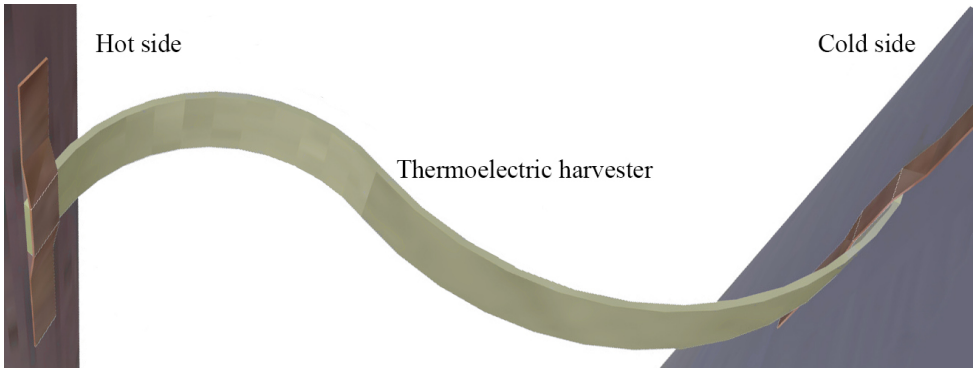

Figure 1.5: Schematic of long metal thermoelectric energy harvester stretched between left side (hot) and right side (cold).

1.4 Piezoelectric harvesters

The gas turbine application calls for a lightweight, broadband energy harvester. With the capability of operation in elevated temperatures, a piezoelectric energy harvester seems like the best choice. Another advantage of building a piezoelectric energy harvester is that most parts needed for the design are available off-the-shelf.

Two piezoelectric harvester types were used, a 2DOF coupled harvester and a self-tuning 4DOF harvester, both designs with focus on broad bandwidth.

1.5 Scope and outline of thesis

Four energy harvesters with varying designs have been developed, two vibrational energy harvesters based on the classified vibrational data acquired from Rolls-Royce PLC®, one thermal energy harvester designed for the cooling channels in the middle to rear of the gas turbine and one metal thermoelectric energy harvester aiming to be simple to design and install.

Paper I and **paper II** covers the analytical modeling, synthesis, assembly and measurements on the thermoelectric energy harvester designed for the cooling channels in a test gas turbine.

As a result of the harvester presented in **paper I** and **paper II** and the challenges of powering a wireless sensor on a gas turbine a second type of thermoelectric design is presented in **paper III**, an all-metal thermoelectric harvester with long reach. The paper covers analytical calculations, assembly, load resistance measurements and powering of two different types of wireless sensor systems.

For the piezoelectric energy harvesters, the design and assembly of coupled harvesters is the main contribution, with most of the parts bought off-the-shelf. In **paper IV** the simulation and experimental validation of a coupled piezoelectric energy harvester is demonstrated and in **paper V** the concept is investigated further with optimizations, cantilever designs and load

resistance measurements. In **paper VI** a simplified finite element analysis of a 4DOF coupled harvester with self-tuning capabilities is presented with experimental verification of the analysis.

The temperature inside a gas turbine reaches above the capabilities of power electronics and wireless sensor systems available. Hence, harvesters located in high temperatures cannot be completely wireless. Construction of a completely wireless sensor is therefore out of scope for this thesis. Also, the harvester in **paper I** has no power measurements, and needs proper solutions to reduce contact resistance first. Due to lack of time and facilities this is deemed out of scope.

The thesis covers the theoretical parts of the harvesters in Chapter 2, followed by the methodology of simulations, measurement setup and measurements in Chapter 3. Results are presented in Chapter 4 with the last chapter devoted to discussion and conclusions.

CHAPTER 2

Energy harvesting in gas turbines

Energy harvesting for wireless sensing is application-specific and it is unreasonable to assume that all energy conversion methods in general can be used for wireless sensors. Likewise, are energy harvesting in gas turbines not equal to energy harvesting in general.

The most notable difference is a strict safety requirement, with limitations on what materials, electronics and designs that are allowed. Also, the environment inside a gas turbine is harsh; the number of sensors can reach thousands in one test gas turbine and with many of the locations needing non-intrusive harvesters as well.

2.1 Thermoelectric harvesters

Even though the Seebeck effect was discovered already in 1820 [70] the use of thermoelectric energy conversion has been limited to very few applications due to the low efficiency. However, with IoT (internet of things), increased use of wireless sensors and more efficient thermoelectric materials it has been placed in the spotlight again. These new thermoelectric materials can reach efficiencies around 13-15% at 1000°C with theoretical efficiencies up to 25% [71]. Because thermoelectric generators are solid state, they can be made very small and keep most of the efficiency [72]. The solid state also gives the harvester high durability and longevity, with more than 30 years of power generation possible [64, 65, 73].

A thermoelectric harvester inside a gas turbine need to survive the vibrations. This can be challenging for high temperature harvesters because of the sometimes brittle nature of the materials. However, if the harvester accidentally comes loose and goes into the turbine blades it should shatter on impact with the turbine walls/blades. If the material is too durable and deforms it could damage the turbine blades (with possible catastrophic failure as a result).

Thermoelectric harvesters require a temperature gradient to generate power, in gas turbines there are several options where to place the harvesters. Active cooling is abundant and includes oil cooling, low temperature exhausts and high-pressure air cooling.

Seebeck effect

The Seebeck effect is one of the three thermoelectric effects and explains the heat-to-energy conversion. The Seebeck effect is observed when two dissimilar materials are connected and exposed to a thermal gradient. The result is an electrical potential proportional to the temperature difference which is both temperature- and material dependent, called the Seebeck coefficient

(V K^{-1}) [74]. There are n-type and p-type thermoelectric materials, with a negative Seebeck coefficient from excess of n-type charge carriers and a positive Seebeck coefficient from excess of p-type charge carriers [75].

Figure of merit and power factor

Common procedure when developing thermoelectric materials and/or thermoelectric harvesters is to present their ”figure of merit”. The dimensionless figure of merit for a material is defined as $zT = \frac{\sigma S^2 T}{\kappa}$, where S is the Seebeck coefficient, σ the electrical conductivity, κ the thermal conductivity and T the temperature. The zT-value is proportional to the efficiency of the material with a theoretical maximum value, the Carnot cycle efficiency [76], at $zT = \infty$. Unfortunately, the figure of merit is difficult to increase and improving one attribute usually have negative effect on the others [75], furthermore the zT-value is temperature dependent and has an optimal temperature range where the zT is highest, see Fig. 2.1 and 2.2. For a thermoelectric generator containing several thermoelectric materials the figure of merit is denoted by ZT.

For large scale power production, a high ZT-value is crucial in order to compete with other conversion methods [11]. This is however not always the case in energy harvesting. With sufficient cooling available and with a thermal energy source far greater than the thermoelectric harvester can transfer, the efficiency of the harvester becomes less important [77].

The power factor, defined as $\sigma S^2 T$, is therefore sometimes a better quality-measure of thermoelectric materials and thermoelectric harvesters. Especially in gas turbines, where heat energy and active cooling can be bountiful.

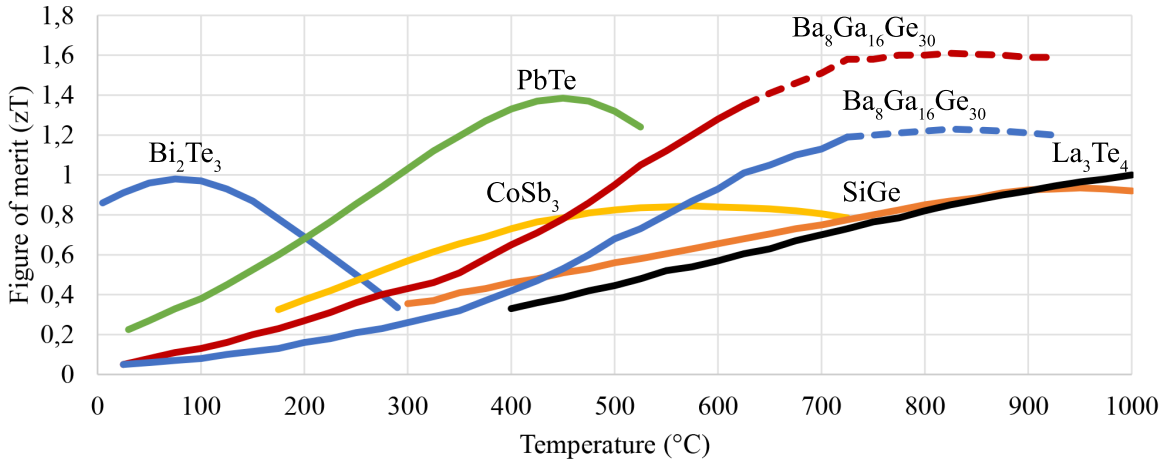

Figure 2.1: zT-value for some common n-type materials between 0-1000°C [75, 78].

2.1.1 Harvester designs

A thermoelectric harvester needs one hot side and one cold side to utilize the Seebeck effect. The shape of the harvester therefore depends on the environment. However, the basic design

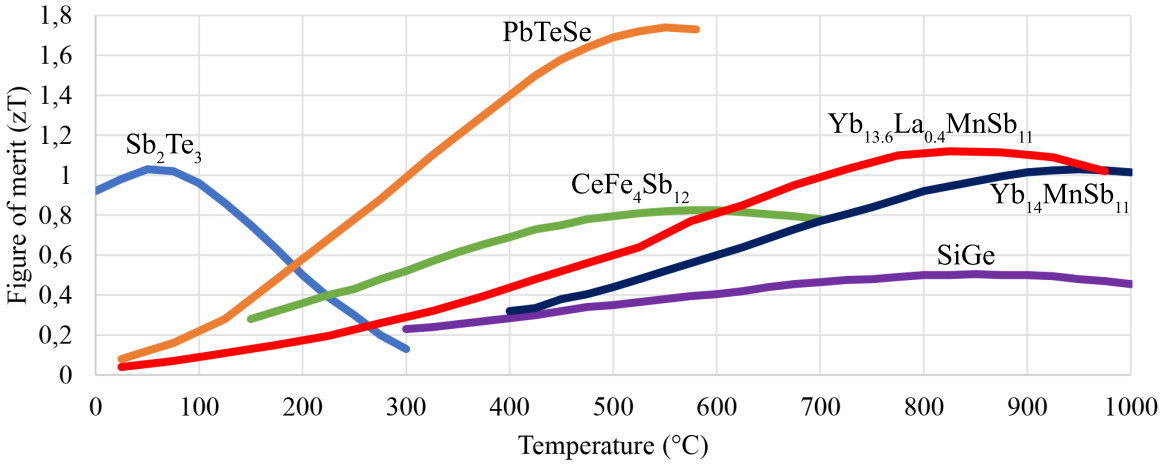

Figure 2.2: zT-value for some common p-type materials between 0-1000°C [75,79].

features remain the same. Connecting n-type and p-type materials in parallel thermally and in series electrically induces an electrical current when exposed to a thermal gradient, see Fig. 2.3. This combined "couple" produces a potential in the range of tens to hundreds of μV K^{-1}.

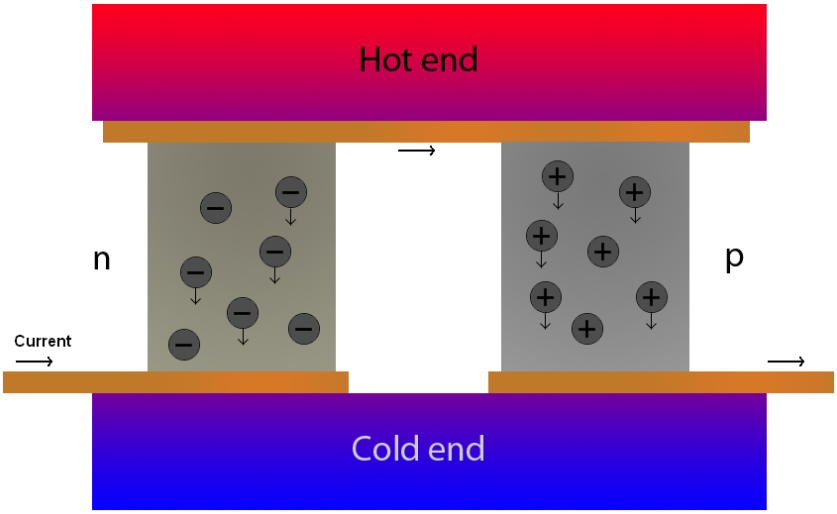

Figure 2.3: Two thermoelectric materials in parallel thermally and in series electrically, current going from left to right and heat from top to bottom.

A thermoelectric generator usually consists of several thermocouples in series to increase the voltage of the device, where each couple consists of one n-type and one p-type leg, see Fig. 2.4. In this type of design, the legs are connected by electrodes placed on electrically insulating and thermally conductive materials. High thermal conductivity in the base plates is important to ensure that enough heat is transferred to and from the thermoelectric legs to maintain a high thermal gradient. Furthermore, the materials should have high zT-value or power factor in the desired temperature range and preferably also have similar thermal expansion coefficient [80].

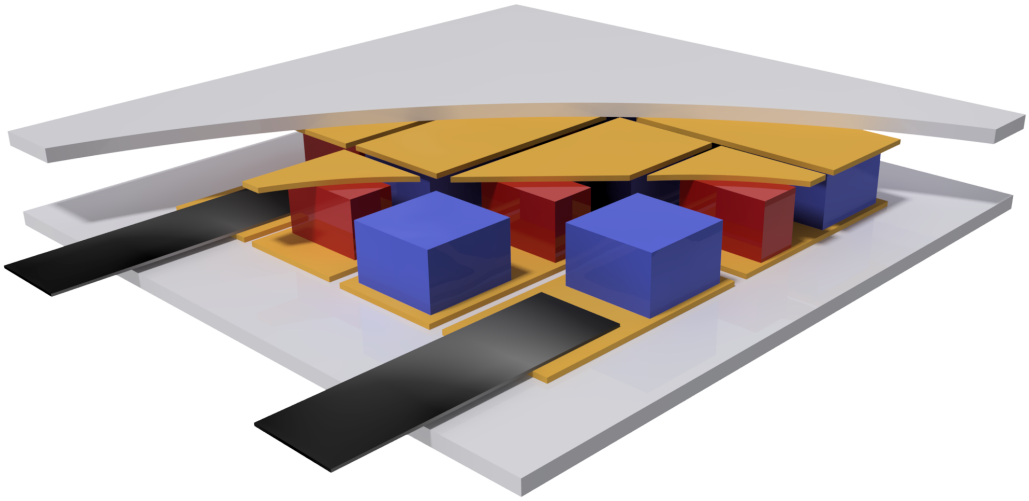

Figure 2.4: Cross section of a thermoelectric device consisting of seven couples between two insulating plates, with the two different materials having different size. A second type of electrode is welded to the electrodes inside the device.

However, when building harvesters that operate at high temperatures (above 600°C) the number of available materials is substantially reduced.

The electrodes can be fitted to the thermoelectric legs in several ways. At low temperature and with insensitive materials it can be soldered or welded. This is not always the best approach, at higher temperatures or with sensitive materials, diffusion bonding can be a better method. In solutions when the electrodes are not bonded physically with the thermoelectric materials, the electrodes and the thermoelectric material need to be pressed together [81]. To reduce stress and ensure connection throughout the device the legs should be even and have the same height at operating temperature. One solution is to use a spring for each leg to even out the force this way [82]. However, using springs is complicated and can affect the thermal conductance through the device and lower the possible maximum thermal gradient substantially.

Voltage, power and efficiency

Because the voltage is generated from the n-type and p-type Seebeck coefficients (V K^{-1}) it is possible to predict the output voltage (open circuit) precisely, if the Seebeck coefficients from both materials are known in the entire temperature span. This is the basis of thermocouple temperature sensors [83]. For a harvester with multiple couples the voltage output can be simplified as in Eq. 2.1 below.

$$V = nS_{avg}T_{diff} \tag{2.1}$$

where n is the number of couples, S_{avg} the average Seebeck coefficient in the temperature range and T_{diff} the temperature difference between the hot- and cold side of the thermoelectric material.

A simplified calculation of the power output (explained in **paper II**) from a thermoelectric

harvester (under load) can be seen in Eq. 2.2 below.

$$P = (nS_{avg}T_{diff})^2 \mu / R(\mu + (1+\delta))^2 \tag{2.2}$$

where R is the resistance of the power-generating portion, μ the load resistance ratio R_l/R and δ the contact resistance ratio R_c/R.

The efficiency (η) of a thermal harvester is simply the portion of the thermal energy that is converted into electric energy, see Eq. 2.3 below.

$$\eta = Q_H/P \tag{2.3}$$

where Q_H is the heat input and P the power output from Eq. 2.2.

Harsh environment

Any environment with high temperatures will cause oxidation on exposed surfaces. The oxidation speed increases with increased temperatures. In a gas turbine, at temperatures above 600°C the materials are dominated by a second type of degradation, hot corrosion. Hot corrosion (molten sulfates) comes from alkali metal contaminants (sodium and potassium) reacting with the sulfur in the fuel [84]. Protecting the energy harvester from degradation in a gas turbine is a major challenge.

The thermoelectric harvester in **paper I** will be placed in locations with these harsh conditions and contains sensitive materials e.g. $Yb_{14}MnSb_{11}$. This material is sensitive to moisture and air and the surface will oxidize even at low levels of oxygen at room temperature. Moreover, the material also reacts with many other materials. $Yb_{14}MnSb_{11}$ is however known to be stable in contact with alumina, graphite and molybdenum [85, 86]. Using Mo or graphite as an electrode material or as protective layer between the electrode material and $Yb_{14}MnSb_{11}$ is therefore possible.

Diffusion can happen where the thermoelectric material meets the electrode or the encapsulating material. Some materials have higher tendency to diffuse than others, so by properly choosing the materials this problem can be reduced. As an example, Sb tends to diffuse into other metals/alloys and form antimonide compounds [87]. In this work Sb is used in the p-type material and the choice of electrode material is therefore crucial. Diffusion can also occur inside the thermoelectric material where single atoms diffuse from their locations. This type of degradation indicates that the temperature is too high for the specific material and a lower temperature or change of material is necessary.

The material that surrounds the thermoelectric legs should have low thermal conductivity, but also keep the sublimation in check. Progress in sublimation repression has been made with alumina paste and is therefore used in this work [85,88,89]. When Yb and Sb starts to sublimate, the Sb flows through the alumina and the material starts to degrade, but the Yb is stopped by the alumina and creates a thin layer of Yb that the Sb cannot pass through. This method that can reduce the sublimation with a factor of 1000.

2.2 Piezoelectric harvesters

Piezoelectric harvesters can handle temperatures up to 300°C if built properly [21] and are thus a possible power source in several locations not suitable for batteries. Commercial piezoelectric cantilevers are more limited with its maximum temperature (150°C) [90], but the principles of the harvesters will work for custom made high temperature piezoelectric harvesters as well.

The cantilevers with piezoelectric material should shatter on impact if released into the gas turbine but metal couplings could damage the blades and should be avoided if possible.

2.2.1 Piezoelectric materials

The piezoelectric effect arises in some materials when exposed to tension and compression and the phenomenon was first published in 1880 [91]. The source of this piezoelectric effect comes from the crystal structure and how the atoms move under pressure to create a dipole moment.

There are many different types of crystal structure that give rise to polarization under pressure [92]. One of the most commonly used is the perovskite structure e.g. lead zirconate titanate, $PbZr_{0.5}Ti_{0.5}O_3$ (PZT).

PZT is also ferroelectric which means that below a certain temperature (Curie temperature) the material has a spontaneous polarization. Above the Curie temperature the material loses its piezoelectric properties [93]. The spontaneous polarization happens in groups of unit cells and is called Weiss domains [94]. The Weiss domains have random polarization vectors and the average polarization in the material is zero if cooled down without any external electric fields.

When fabricating a piezoelectric material for energy harvesters the Weiss domains are forced in the same direction by applying an electric field when the temperature is slightly below the Curie temperature. This treatment is called poling and will slightly deform the material to be anisotropic and give it a permanent polarization.

2.2.2 Amplification and bandwidth

The basic concept of vibrational harvesters is to match the self-resonance frequency of the harvester with the vibrations in the environment to amplify the response in the harvester. This amplification can be made very efficient and reach a factor 200 or more, under the condition that the mass of the environment is far greater than the mass of the harvester [95]. The amplification can be expressed with a quality factor (Q) seen in Eq. 2.4 below.

$$Q = \frac{2\pi E}{\Delta E} \tag{2.4}$$

Where E is the stored energy and ΔE the energy lost each cycle. If the damping is low, the same quality factor can also be expressed as in Eq. 2.5.

$$Q \approx \frac{\omega_{res}}{\Delta\omega} \tag{2.5}$$

where ω_{res} is the resonance frequency (Hz) and $\Delta\omega$ the bandwidth (Hz) [96]. A high quality factor means low losses and high amplification (which of course is a good thing) but it also gives a narrow bandwidth.

Without revealing any classified gas turbine vibrational data, it can be stated that a wider bandwidth is needed than a single cantilever can achieve.

2.2.3 Harvester designs

A piezoelectric accelerometer is built to absorb all vibrations equally [97]. This requires that the accelerometer never reaches its resonance frequency because of the amplification created by self-resonance. For a piezoelectric energy harvester, the ambition is to have as much amplification as possible. Inspecting the vibration spectrum of the environment gives information on how to design the harvester to have the resonance frequency matched with the most energetic vibrations in the environment.

The basic design of a piezoelectric energy harvester is a cantilever with a thin layer of piezoelectric material on one or both sides of the cantilever. For a single degree of freedom (SDOF) system the undamped natural frequency is expressed as follows in Eq. 2.6.

$$\omega_0 = \sqrt{\frac{k}{m}} \tag{2.6}$$

Where ω_0 is the undamped natural frequency, k the effective stiffness of the system and m the effective mass. With the added damping of the system the resonance frequency is expressed as in Eq. 2.7 below.

$$\omega_{res} = \omega_0 \cdot \sqrt{1 - 2\zeta^2} \tag{2.7}$$

If the resonance frequency of the environment is fluctuating or changing in some way, a single cantilever could get off resonance with low power output as a result. Increasing the bandwidth of the piezoelectric harvester to cover the resonance frequency span of the environment is therefore important.

Coupled energy harvester

With two single cantilevers it is possible to cover two different frequencies, either by two different types of cantilevers, lengths or by introducing a tip mass, see Fig. 2.5. Two single cantilevers can therefore give double power output at one resonance frequency or approximately double bandwidth depending on the tuning of the cantilevers.

Connecting one cantilever to the end of another cantilever will give a different scenario, see Fig. 1.4. This design will naturally have two different resonance frequencies for the two cantilevers with a complicated relationship between them.

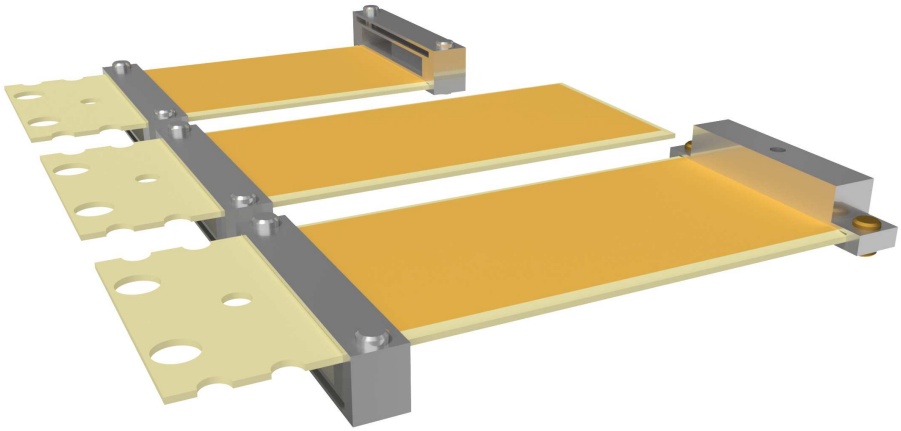

Figure 2.5: Three single cantilevers with different eigenfrequencies. Longer length and introduced tip-mass lowers the eigenfrequency.

Self-tuning energy harvester

It is possible to increase the bandwidth of a harvester with self-tuning abilities. This work connects a dual clamped beam between two single cantilevers in a similar fashion as the coupled harvester, see Fig. 2.6. This setup will give two resonance frequencies, one for each cantilever.

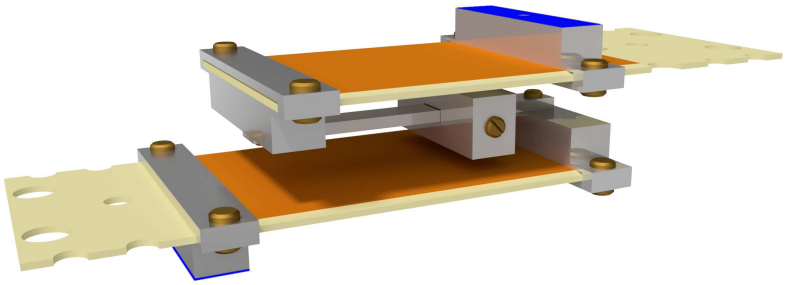

Figure 2.6: Self-tuning harvester with two cantilevers and one beam connecting them. A sliding mass is attached to the beam. The two fixed points are marked in blue.

With a simplified finite element analysis of the system it is possible to derive computationally efficient codes or even closed form solutions that enable comprehensive investigations of variation in geometrical and material parameters. This simplified model can be seen in **paper VI**. The system is studied using Euler-Bernoulli theory for isotropic beams with additional point masses [98]. In **paper VI**, the electromechanical coupling effects for the piezoelectric cantilevers are neglected as they are of minor importance for the overall structural eigenfrequency response. Moreover, the laminated structures of these beams are modelled as homogeneous beams using effective material properties. As for the sliding mass, it is assumed to be fixed at various positions along the middle beam. This assumption simplifies the analyses considerably while having little effect on the system's eigenfrequency.

CHAPTER 3

Simulations and fabrication of energy harvesters

The thermoelectric and piezoelectric harvesters were designed and assembled with the aim of gas turbine applications, more specifically stationary gas turbines in test facilities. The extra amount of sensors in these gas turbines increased the need for wireless sensing.

3.1 Semiconductor harvester

The middle part of the gas turbine was one of the most challenging locations to replace wired sensors with less-wired sensors. In the test gas turbine at Rolls-Royce PLC®, the wall temperatures reached 800-900°C in the areas with active cooling, with cooling air temperatures reaching 500-600°C, giving a potential thermal gradient of 200°C or more. The cooling channel location also introduced size constraints on the harvester at approximately 1-2 cm^2 and a few mm in height with the heat sink included. The aim was a power output of 1 mW for this harvester.

Design boundaries

The design choice was a standard thermoelectric design with two semiconductor thermoelectric materials connected in series electrically and in parallel thermally, squeezed between two base plates.

3.1.1 Analytical optimization

Because of that the conversion efficiency of thermoelectric materials are temperature dependent and the environment had the unusual temperature span (600-800°C) an analytical model was made to assess what materials were most suitable, see **paper II**. The analytical calculations also helped with design optimization and to predict characteristics of the harvester.

For this particular gas turbine application [2] the aim for weight and size of the device was approximately 0.5-1 grams and 1-2 cm^2. Due to the size constraint, all the materials inside the harvester were included in the calculations to get an approximation of thickness, weight and an indication of where problems could arise during assembly. It was important to include the temperature dependent material properties (e.g. electrical resistivity and thermal conductivity) in the calculations. An example was the alumina used as base plate material that have a thermal conductivity of about 7 W $m^{-1}K^{-1}$ at 800°C and 37 W $m^{-1}K^{-1}$ at room temperature [99]. SiC has a thermal conductivity of 48 W $m^{-1}K^{-1}$ at 800°C as comparison.

The calculations made it possible to get some first estimations of the heat transfer and power output of the device. Because of the complexity and the number of variables the calculations were an iterative process. Variables included number of couples in square devices (n=1, 3, 7, 11, 17, 23, 31...), height of thermoelectric legs, area of legs, thermal gradient of environment, thermal conductance of base plates, area ratio between n-type and p-type material, thickness of electrodes, electrode resistance, load resistance, parasitic heat conductance between couples and different thermoelectric materials, base plate materials, sealant materials and electrode materials. These variables were then tuned to optimize the specific power output (W/kg), with high temperature cables [100] to the power management included. The electrical and thermal contact resistance ratios were set to 0.1 and 0.2 of the total harvester resistances, as this was appropriate values in commercial harvesters [101]. By including all these parameters, it was possible to get some predictions on the power output and the important design parameters. An example can be seen in Fig. 3.1, where the number of couples are reduced from 17 to 1. The increased percentage losses from cables, load resistance and DC-DC conversion (80% efficiency vs 30% efficiency) reduced the power output from 450 mW to 1 mW (with 2.5 Ω load resistance).

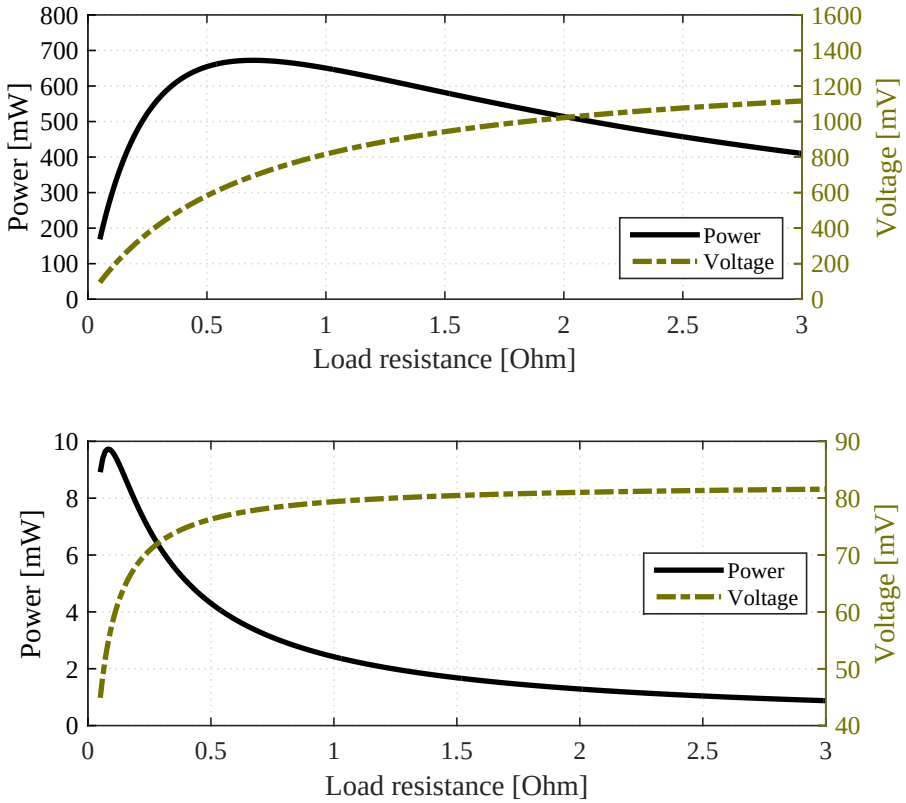

Figure 3.1: The power output and voltage of a 17-couple harvester (top figure) and 1-couple harvester (bottom figure) as a function of the load resistance after losses in cables and DC-DC converter.

The height of the legs had the highest effect on the power output and reducing the leg height resulted in higher power output and lower efficiency, see Fig. 3.2. However, to keep the heat

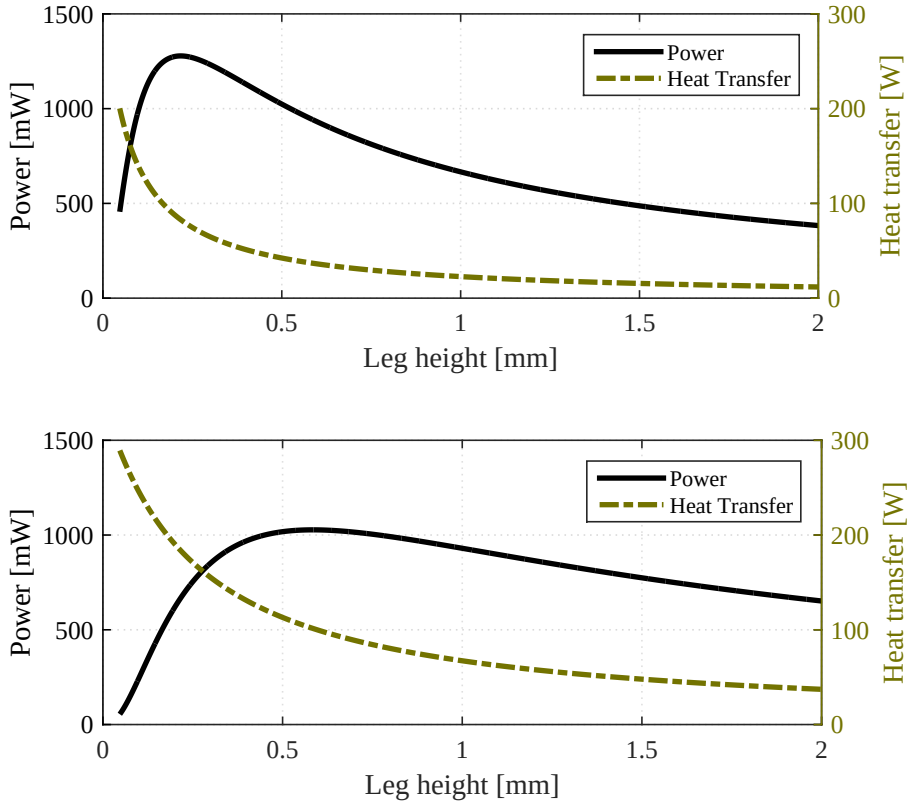

Figure 3.2: Top picture: Power output and heat transfer as a function of leg height for $Ba_8Ga_{16}Ge_{30}$ and $Yb_{14}MnSb_{11}$. Bottom picture: Power output and heat transfer as a function of leg height for SiGe.

sink at a reasonable size the maximum heat input had to be limited according to Eq. 3.1 [102] below.

$$P_D = \frac{T_J - T_A}{\theta} \tag{3.1}$$

A junction temperature (T_J) at 600°C, a cooling air temperature (T_A) around 500°C and a thermal resistance of 4°C W^{-1} equals a power dissipation (P_D) of 25 W. The estimated thermal resistance of 4°C W^{-1} could be achieved with a heat sink size of 12 mm × 12 mm × 3 mm [103] without constricting air flow to much in the cooling channels, see Fig. 3.3. Please note that in this case, without any detailed measurement data available about size of channel, pressure and airflow velocity inside the cooling channels the thermal resistance of 4°C W^{-1} could be a rough estimation.

One challenge when building a 12 mm × 12 mm thermoelectric harvester was the number of couples that can fit inside. Increasing the number of legs increased the voltage, which was important, but it also made the device assembly more complex. And with insulating material or diffusion suppressing material between the legs or electrodes the total volume of thermoelectric material decreased with more couples. In this regard the choice of materials was of big importance as will be explained in the following section.

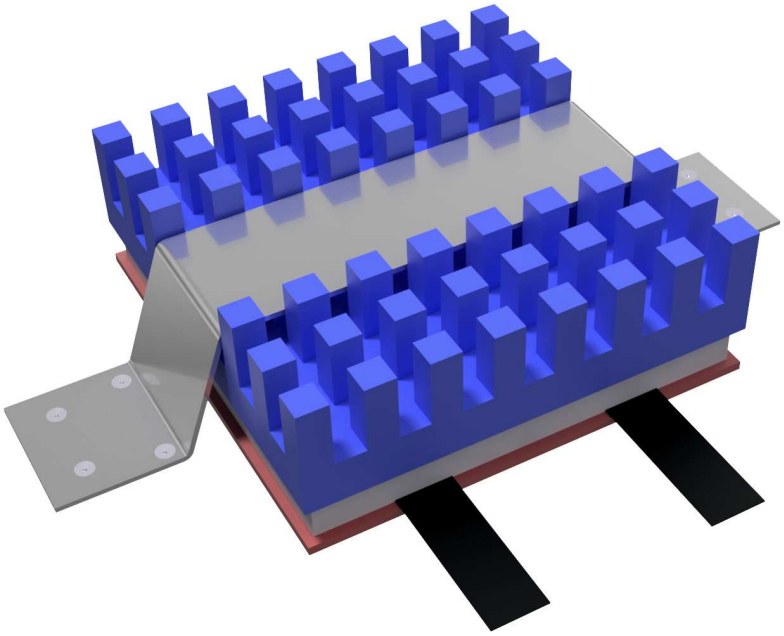

Figure 3.3: Thermoelectric harvester including heat sink and metal holder.

Material choices

To choose the materials in this project the analytical model was used in conjunction with assembly-crucial properties, such as thermal expansion, diffusion- or sublimation suppression. Increasing temperature will affect materials in various ways, like oxidation, sublimation and diffusion. Thermoelectric materials in temperatures as high as 800°C can degrade quickly if not properly cared for. Oxidation can be reduced by proper encapsulation of the device and the individual legs. Finding a suitable encapsulation is however difficult due to possible degradation of the encapsulating material itself and the fact that the encapsulating material will have a parasitic effect on the harvester, since the material will transfer heat energy through the device.

From calculations the thermoelectric materials $Ba_8Ga_{16}Ge_{30}$ [78,104] and La-doped $Yb_{14}MnSb_{11}$ [79] gave the best results in the temperature range (600-800°C). The materials figure of merit can be seen in the comparison of different thermoelectric materials, see Fig. 2.1 and 2.2.

Using a synthesis procedure covered in **paper I** the n-type material was synthesized with a highly crystalline material as a result. The melting point of $Ba_8Ga_{16}Ge_{30}$ (approximately 966-974°C) sets the absolute upper temperature limit of the device. The figure of merit for this material is high and at 700°C values above 1.2 has been reported with Seebeck coefficient of -220 μV K^{-1}, electrical resistivity at 17 $\mu\Omega$m and thermal conductivity at 1.25 W m^{-1}K^{-1} [78]. The thermal expansion is quite high at 14.2 μm K^{-1} [105].

In **paper I** the synthesis of the p-type material gave less abundant results with some Sn residue left on the crystalline material. The figure of merit for the La-doped $Yb_{14}MnSb_{11}$ has been reported as high as 1.2 with a Seebeck coefficient of 200 μVK^{-1}, electrical resistivity $7.5{\cdot}10^{-5}$

Ωm and thermal conductivity at 0.6 W $m^{-1}K^{-1}$ [79]. The thermal expansion is higher than $Ba_8Ga_{16}Ge_{30}$ at 16-17.9 μm K^{-1} [106, 107].

$Yb_{14}MnSb_{11}$ sublimates and Mo-electrodes oxidizes at high temperatures. Consequently, the harvester was fabricated in an oxygen free environment (argon filled glove box) and later also sealed with ceramic glue to not let oxygen or moisture through. Furthermore, alumina paste (Thermeez 7020) [108] was placed around the thermoelectric materials to reduce sublimation [85]. The thermal conductivity of Thermeez 7020 is 0.159 W $m^{-1}K^{-1}$.

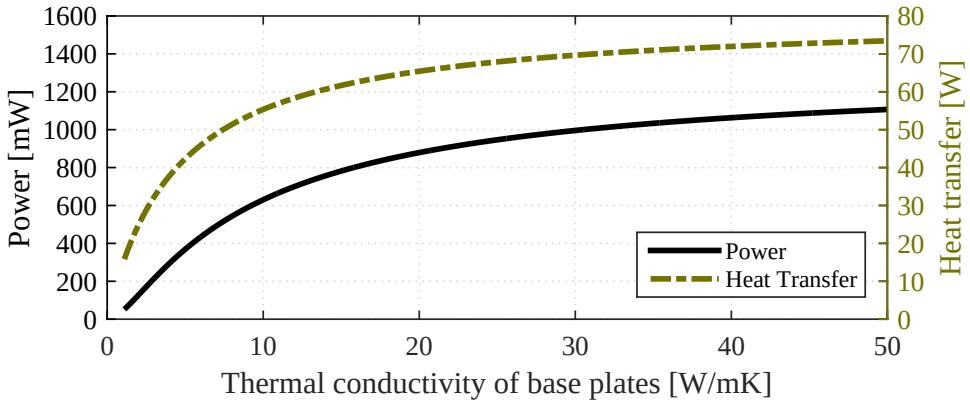

Figure 3.4: Power output and heat transfer through the SiGe generator with increasing thermal conductivity in the base plates.

The thermoelectric harvester design had two electrically insulating base plates, see Fig. 2.4. At 800°C the best choice would be SiC with 48 W $m^{-1}K^{-1}$ and high durability, compared to a more brittle alumina with a thermal conductivity of 7 W $m^{-1}K^{-1}$. But with a cost of more than 10 times that of alumina, calculations were made to see if the higher price would pay off. If using SiGe as thermoelectric material a 0.25 mm thick SiC base plate would be a good choice because of the high thermal conductivity of SiGe, see Fig. 3.4. The high thermal conductivity of SiGe also pushed the heat flux beyond the recommended 25 W allowed by the heat sink, with possible low thermal gradient over the thermoelectric legs as a result.

However, with the low thermal conductivity in $Yb_{14}MnSb_{11}$ and $Ba_8Ga_{16}Ge_{30}$ the heat transfer stayed below 25 W and with alumina sheets as thin as 0.25 mm the difference was only 4 % lower power output compared to SiC, see Fig. 3.5. Increasing the thickness to 1 mm would reduce the power output by approximately 17 % with alumina base plates compared to SiC.

Another aspect of using SiC would be the durability and improved thermal shock resistance. The alumina plates can crack from thermal shock [109] with destroyed harvesters as a result. The improved durability could however be dangerous if the harvester would come loose and hit a turbine blade.

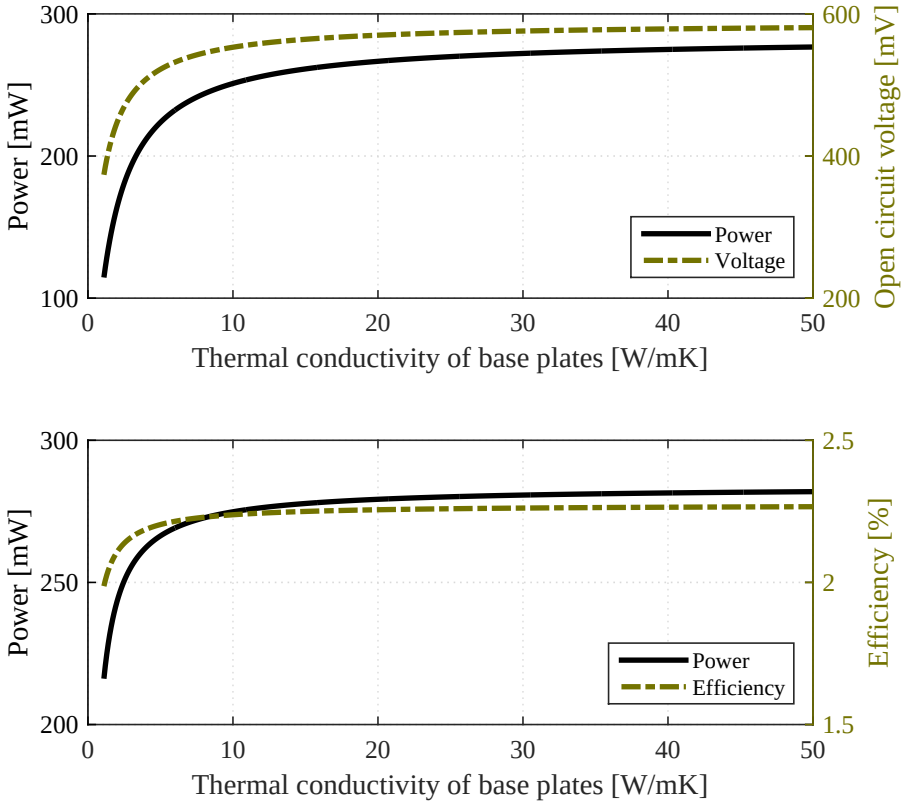

Figure 3.5: The power output and efficiency of a 7-couple harvester as a function of the thermal conductivity of the base plates. Top: 1 mm thick base plates. Bottom: 0.25 mm thick base plates.

Thermoelectric leg size

The size of the legs was determined by the material choices with an optimum area-ratio of 1:3.7 for $Ba_8Ga_{16}Ge_{30}$:$Yb_{14}MnSb_{11}$. However, cutting the legs was the ultimate size restriction. When cutting smaller than 1 mm the legs broke or chipped too frequently, and the height of the leg was therefore forced to a minimum value of 1 mm.

The smallest area that could be achieved now depended on the internal stress from thermal expansion. A 200°C temperature gradient over 1 mm required a leg width of 1.6 mm to avoid fracture from internal stress for the n-type material [105]. Therefore, the area-ratio was set to 1:1 with 13% reduction in power output as a result.

3.1.2 Harvester assembly

Because of the sensitive thermoelectric materials, the harvester had to be assembled in an argon filled glove box. The $Ba_8Ga_{16}Ge_{30}$ was relatively stable after synthesis, but this was not the case for the $Yb_{14}MnSb_{11}$.

The assembly of a 1-couple proof-of-concept harvester is explained in **paper I**. The materials used was $Yb_{14}MnSb_{11}$ and $Ba_8Ga_{16}Ge_{30}$ with 1:1 area-ratio, molybdenum electrodes, alumina base plates, alumina (Thermeez 7020) insulation and Inco600 electrodes spot welded inside the module. The module was sealed with two different ceramic glues.

The base plates had the purpose of build platform and to transfer heat to the thermoelectric material from the surroundings. Alumina is a hard, electrically insulating, inexpensive material with moderate thermal conductivity and can be made very thin. The alumina substrates were delivered in 50 mm x 50 mm plates with a thickness of 0.254 mm.

When cutting the thermoelectric materials, the strategy was to cut pieces small enough to fit 17 couples in 1.44 cm^2 and still have some room for insulation and sublimation barrier between the legs. Cutting the $Ba_8Ga_{16}Ge_{30}$ to the desired size proved difficult, with fragments chipped of the corners, destroying the legs. With limited amount of La-doped $Yb_{14}MnSb_{11}$ and with the risk of exceeding the area-to-height ratio for internal stress, the decision was to cut both the La-doped $Yb_{14}MnSb_{11}$ and the $Ba_8Ga_{16}Ge_{30}$ to a size of 1.6 mm $\times$ 1.6 mm $\times$ 1 mm, see Fig. 3.6. This gave room for approximately 0.5 mm sublimation barrier between the legs in a 17-couple harvester.

To protect the materials from oxygen and moisture during the cutting procedure a coating of wax was applied to the crystals inside the glove box. Also, during the cutting of $Yb_{14}MnSb_{11}$ the cutting fluid was changed from water to hexadecane [110] which produces a protective thin oil coating on the newly cut surfaces of the crystals.

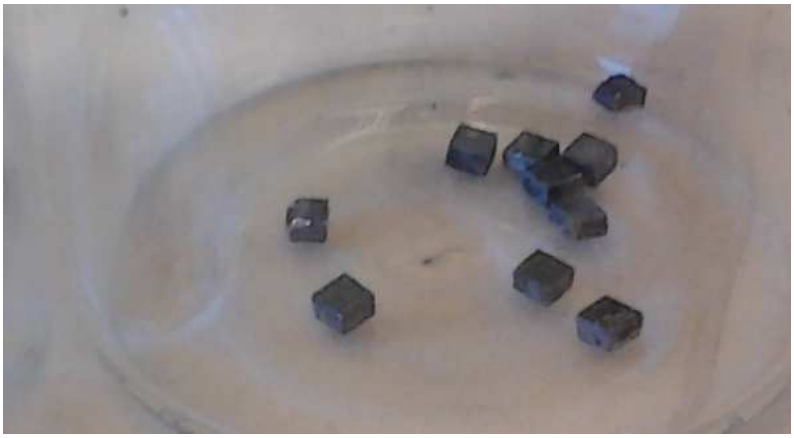

Figure 3.6: The size (1.6 mm $\times$ 1.6 mm $\times$ 1 mm) of the thermoelectric legs in the harvester. The material in this picture is $Ba_8Ga_{16}Ge_{30}$.

To seal and protect the materials from oxygen the harvester was encased in two different kinds of ceramic glue (Renolit 762 and Thermic 1100) capable of creating a gas impermeable seal up to 800°C respectively 1100°C [111, 112]. The inner glue (Thermic 1100) was applied and cured inside the Argon filled glove box and the Renolit 762 was applied outside the glovebox. Both glues are water soluble but should maintain the seal under normal conditions given that the Renolit 762 compound was approved and used frequently by both Rolls-Royce PLC® and GKN Aerospace.

The thermoelectric legs were separated by a ceramic grid made out of alumina. In Fig. 3.7.1a the ceramic grid can be seen with dummy-legs inside. The ceramic grid was built from a water-based paste (Cotronics Thermeez 7020) which when cured was unsolvable in water [108]. The alumina can operate at up to 1100°C and should act as a sublimation barrier for $Yb_{14}MnSb_{11}$ [85]. The ceramic grid made it easier to assembly the device and acted as a glue to keep the harvester intact during assembly. The ceramic grid was made by curing the ceramic paste in a PTFE (Polytetrafluoroethylene) mold pressed against a base plate, see Fig. 3.7.1b.

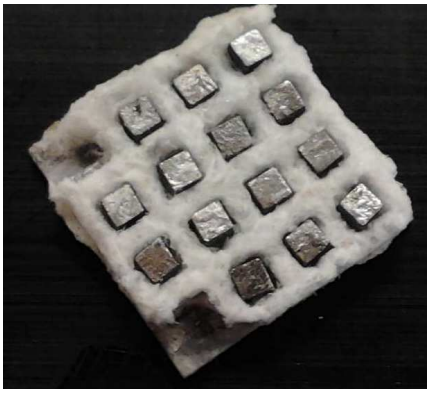

3.7.1 (a) 7-couple ceramic grid made to make assembly easier. The legs in this picture are a bit smaller than the legs used in the actual devices.

3.7.1 (b) PTFE mold with an area-ratio of 1:2.6.

Electrodes

The electrodes were placed on the alumina plates and connected electrically through the thermoelectric materials. Due to time constraints and lack of facilities to handle the sensitive p-type material, the electrodes were not bonded properly with the thermoelectric materials. The electrodes could not be placed exactly flat and the legs was neither perfectly flat nor of the exact same height. The solution was to make electrodes on one side that could act as compression springs as well, see Fig. 3.7.2. The molybdenum was covered with a thin graphite layer in order to improve thermal and electrical contact resistance.

Figure 3.7.2: A schematic figure showing an electrode that has been shaped to act as a spring during first heating. The electrode has some spring force left even when pushed flat.

Most of the compression of the spring electrodes were permanent, when compressing from 0.5

mm thickness to 90 μm it retracted back to 190 μm. The measured difference of the height of the legs was below 50 μm. With the 25 μm graphite sheet to plastically deform under pressure, the force required for good electrical connection was noticeably reduced.

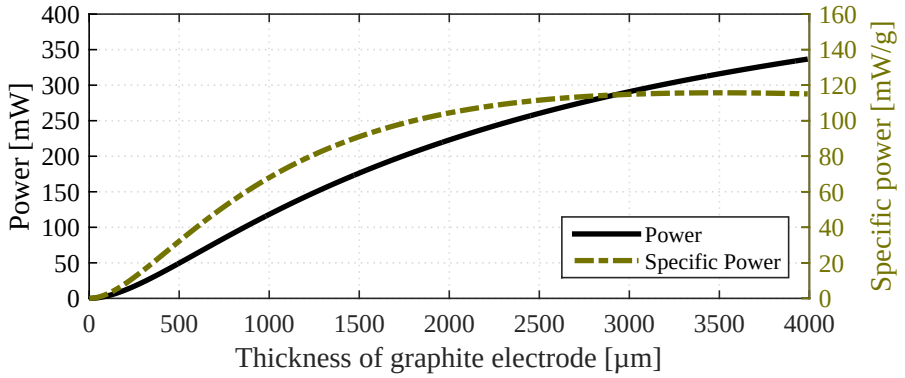

Figure 3.8: The power output and specific power of a 17-couple harvester as a function of the thickness of the graphite electrodes.

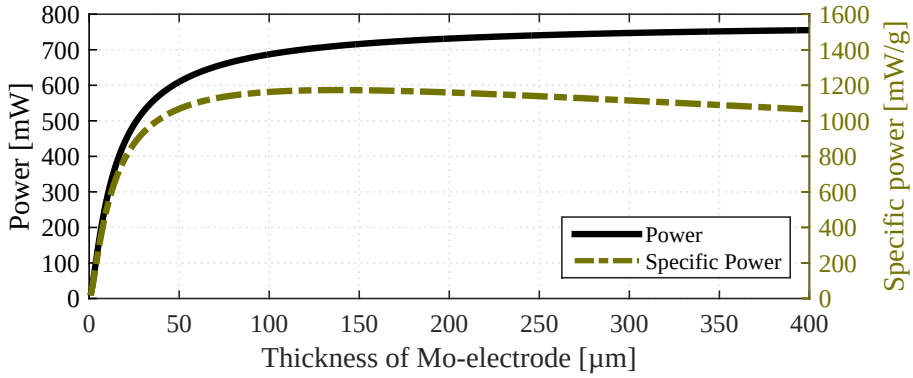

Figure 3.9: The power output and specific power of a 17-couple harvester as a function of the thickness of the Mo-electrodes.

Because of the p-type material the electrode material was limited to graphite, Mo or Mo-coated material [85]. Graphite electrodes would have simplified the fabrication process compared to molybdenum electrodes with better thermal and electrical contact between the thermoelectric material and the electrode as well as having a less violent reaction to oxygen in high temperatures compared to molybdenum [113]. However, with a much lower electrical conductivity and the low thermal conductivity in the c-axis [114] the electrode would need to be thick (highest specific power with 2500-4000 μm), see Fig. 3.8. This would make the device thickness approximately 4-6 mm thicker than for the Mo-electrode device and therefore above the weight and size limit. Calculations based on molybdenum as electrodes, with resistivity of 220 nΩm at 700°C [115] showed optimum electrode thickness at 130 μm for power to weight ratio, see Fig.

3.9.

Connecting cables directly to the Mo-electrodes could be done by spot welding but because of the volatile oxidization of Mo this had to be done before closing the device. A more elegant solution that made it possible to seal the device before attaching cables was to spot weld a less sensitive material (Inco600) to the Mo-electrode, see Fig. 3.10. This enabled the harvester to be sealed with two electrodes out of the harvester.

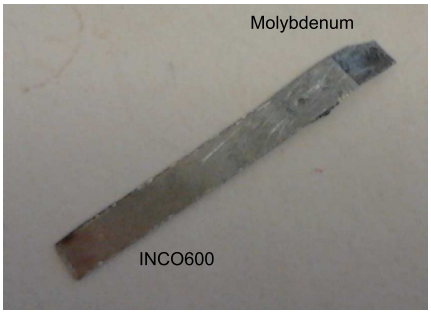

Figure 3.10: Spot welded Inco600 on Mo-electrode.

The cables were prepared at GKN Aerospace in Trollhättan for this project. One cable contains two thin nickel-plated copper wires, these wires are insulated with MgO, has an outer shell of stainless steel [100] and are sealed at the ends with glass. The glass seal is essential to protect the insulation from moisture.

3.2 All-metal harvester

The all-metal thermoelectric harvester had a different approach than the semiconductor thermoelectric harvester. The difficulties met with electrode contacts, limited heat transfer, sensitive materials and load resistance match was the background to why the all-metal harvester was developed. The aim of this harvester had more emphasis on the complete wireless sensor system, with a non-intrusive design that requires little-to-no high temperature cables to connect to electronics.

The required voltage output for the wireless sensor electronics (CC2530 ZigBee development board [57] and LoLin NodeMCU V3 (ESP8266) [116]) was approximately 3.3 V and the required start-up power requirement 10.2 mW over 850 ms (8.7 mJ) for the CC2530 platform [117] and 200 $\pm$(50) mJ (measured) for the NodeMCU platform. These requirements needed to be included from early design level. The voltage and power output from the metal harvester did not reach these requirements and needed power management electronics to convert the low voltage and supercapacitors to store enough energy to manage the start-up requirement. The power management electronics (LTC3108) was included in the analytic model as well.

3.2.1 Analytic analysis

Two different metal harvester designs were investigated, one short (55 mm) 3-couples harvester with just enough voltage to power the LTC3108 electronics and one long (300 mm) 10-couples harvester to reach active cooling far away. Both harvesters were made of 110 μm thick molybdenum foil and 150 μm thick nickel foil.

Increased length of the harvester increased the internal resistance and reduced the heat transfer through the harvester. The calculations estimated the power output of a 10-couples harvester to 4900 μW (37 mV) at a length of 55 mm, reduced to 900 μW (37 mV) with 300 mm length, see Fig. 3.11.

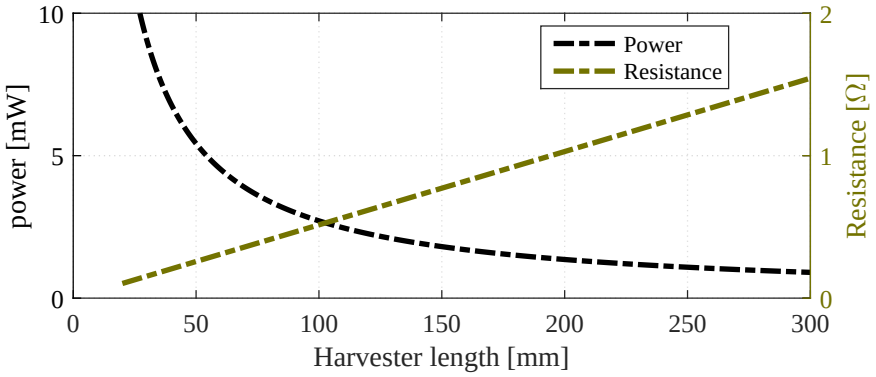

Figure 3.11: Calculated power output in mW (black dashed line) and resistance in Ω (yellow dashed line) from a 10-couples harvester, as a function of the harvester length.

3.2.2 Harvester Assembly

Two harvesters were assembled using the same metal foils. The short 3-couples harvester with 55 mm length and 6 mm width and the long 10-couples harvester with 300 mm length and 3 mm width. The short harvester foils were separated by polyimide tape on the cold side and glass fiber on the hot side, see Fig. 3.12.

The glass fiber insulation was difficult to implement over distances longer than 10-20 mm, with full polyimide insulation for the long harvester as a result. The method of joining the metal foils were the same for both harvesters, by spot welding the metals together in a zigzag pattern, see Fig. 3.13.

The short harvester foil width of 6 mm left more room for welding and the short harvester had 4 welding spots per joint while the long harvester with 3 mm width only had one welding spot per joint.

Figure 3.12: Assembled 55 mm harvester from Ni and Mo foil spot welded together, insulated with polyimide tape on the cold side and glass fiber on the hot side.

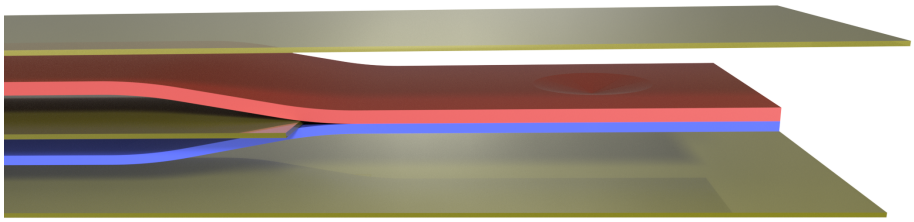

Figure 3.13: Schematic of metal harvester with two thin metal foils welded together in zigzag shape.

Spot welding

A spot welder was used to weld the metal foils together. The spot welder was built from a transformer with 100 turns on the high voltage side and 2 turns on the low voltage side, giving 4.6 V on the low voltage side. The pulses were controlled with a solid-state relay and an ESP8266 circuit [116].

The welding current was not measured, but the power input to the spot welder was measured to 13.8 kVA (60 A at 230 V). Each spot weld was done with two pulses, one 20 ms pulse to soften the metal, a 20 ms pause and then another 40 ms pulse to weld the metals together. The electrode force was constant at approximately 100 N during the welding process with 1.5 mm diameter of the welding electrodes.

3.2.3 Electronics

Two different wireless sensor transceivers were powered with the harvester, CC2530 ZigBee development board [57] and LoLin NodeMCU V3 (ESP8266) [58]. These transceivers required

higher voltage (optimum voltage 3.3 V) than the harvester could achieve, and a power management circuit was added to the system.

Thus, the power management circuit (LTC3108 [54]) was implemented in the system in order to boost the voltage to 3.3 V. The LTC3108 boosted the voltage, starting at 20 mV, to the required 3.3 V. The circuit then stored the energy in a supercapacitor (40 mF) until the voltage in exceeded 3.15 V and the power was released to the wireless sensor transceivers.

3.2.4 Measurement setup

The two metal harvesters were both measured in the same measurement setup with two heater blocks clamping down on the harvester and an ice bath for cooling, see Fig. 3.14.

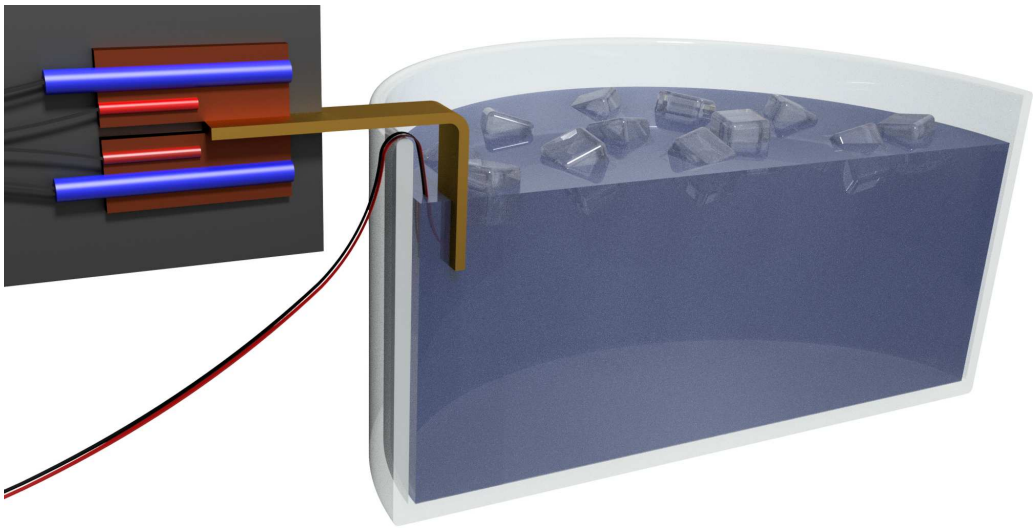

Figure 3.14: Measurement setup of the short harvester clamped between two copper blocks (blue heater elements and red temperature sensors) packed inside insulating material (black block). The cold side was submerged in an ice bath.

3.3 Piezoelectric harvesters

The vibrational data from the test gas turbine (classified) called for a broadband energy harvester with a resonance frequency in the 100-150 Hz span. Two designs were investigated for broader bandwidth harvesting, a coupled backfolded harvester and a self-tuning backfolded harvester, both assembled from off-the-shelf commercial piezoelectric cantilevers [90].

3.3.1 Simulations

Simulations were made in COMSOL Multiphysics for design optimizations and for resonance frequencies tuning [118]. The off-the-shelf cantilever was modeled in COMSOL with a glass epoxy laminate (FR4), piezoelectric material (PZT) and a copper-clad polyimide laminate (Espanex) material.

When designing the harvester, extensive simulations were made with different materials for the couplings and with different lengths and tip masses. The folded design made tuning by hand difficult and simulations were needed for this as well.

Coupled harvester

The coupled harvester consisted of two piezoelectric cantilevers, with the top cantilever fixed on top of the bottom cantilever tip mass directed backwards, see Fig. 3.15. With the centre of mass closer to the fixed point, the folded design produced a lower resonance frequency on the bottom cantilever compared to a non-folded design.

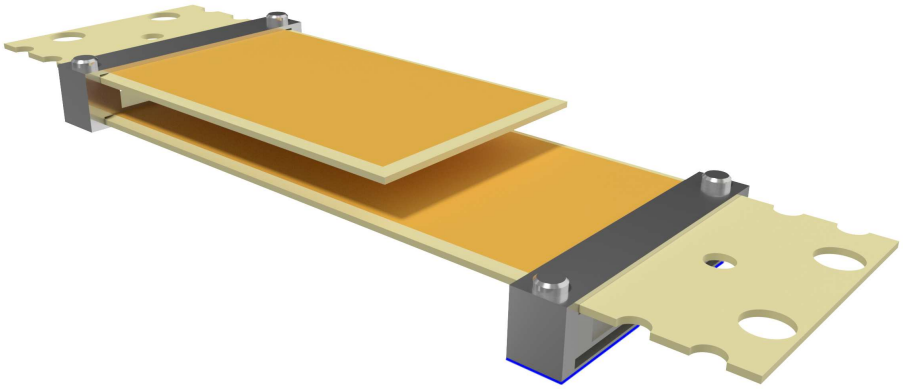

Figure 3.15: Coupled harvester with the shorter top cantilever folded backwards.

The harvester in **paper IV** was simulated and assembled with PTFE couplings. The simulations showed that the coupled harvester not only increased the bandwidth but also gave increased power output compared to single cantilevers.

One explanation for the increased power output could be the added mass to the bottom cantilever from the top cantilever. The folded design added a large mass (the top cantilever) to the bottom cantilever while still maintaining a relatively high resonance frequency. From inspection of the first resonance mode, with the bottom cantilever in resonance, the coupled design had a more even stress distribution over the piezoelectric material, see Fig 3.16a. In fact, the stress distribution on the bottom cantilever could be made almost even in the simulations. The top cantilever had less stress than a single cantilever but with similar shape in the stress distribution with high stress at the fixed point, reduced over the length of the cantilever.

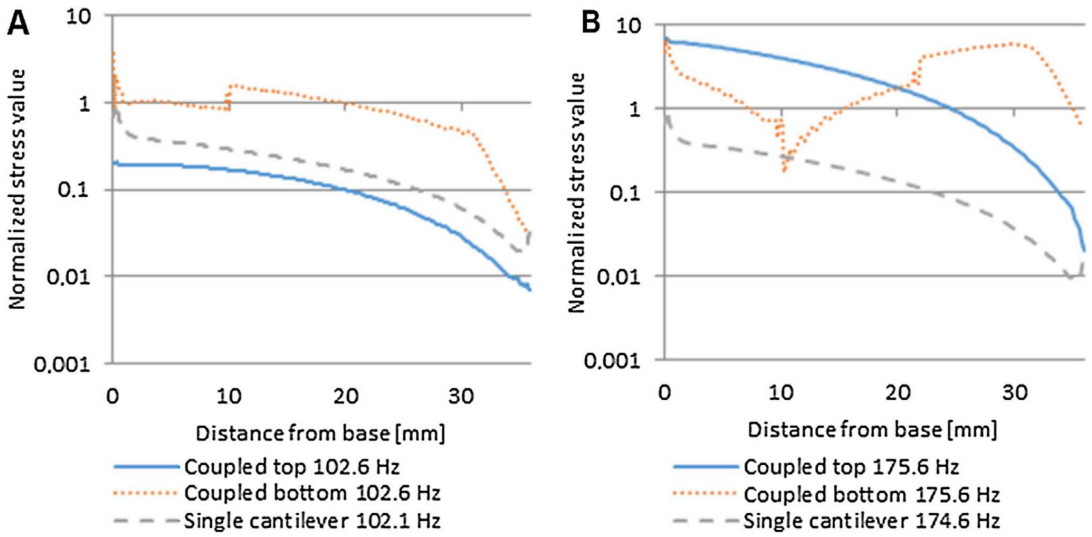

Figure 3.16: Comparison of stress distribution between a single cantilever (grey dashed line), the coupled bottom cantilever (orange dotted line) and the coupled top cantilever (blue solid line). Picture A show the first mode of resonance and B the second mode resonance.

The second resonance mode, when the top cantilever was in resonance, showed an even stress distribution for the bottom cantilever but in this case the bottom cantilever gave close to zero power output because of the s-formed shape of the cantilever, see Fig 3.16b and **paper IV**. The power output was however still higher than from the two single cantilevers and with wider bandwidth.

3.3.2 Fabrication

The harvesters presented in **paper IV**, **paper V** and **paper VI** were all assembled from off-the-shelf piezoelectric cantilevers [90]. The design and the materials used in **paper IV** aimed to keep the harvester approved for use in locations on the gas turbine where it would not damage the gas turbine insides if it were to come loose. This meant PTFE couplings and PTFE screws.

Paper V focused more heavily on experimental results and several different couplings, lengths and cantilever hole patterns were investigated. Even though it could limit the amount of possible harvester locations, in this work the couplings were made of aluminium, because of the unwanted damping seen with the use of PTFE couplings.

The self-tuning harvester (**paper VI**) had the most complex assembly and required a frame in aluminium to keep the two clamping points fixed in relation to each other, see Fig. 3.17. Additionally, the harvester measurements in **paper VI** mainly focus on verifying the analytical model.

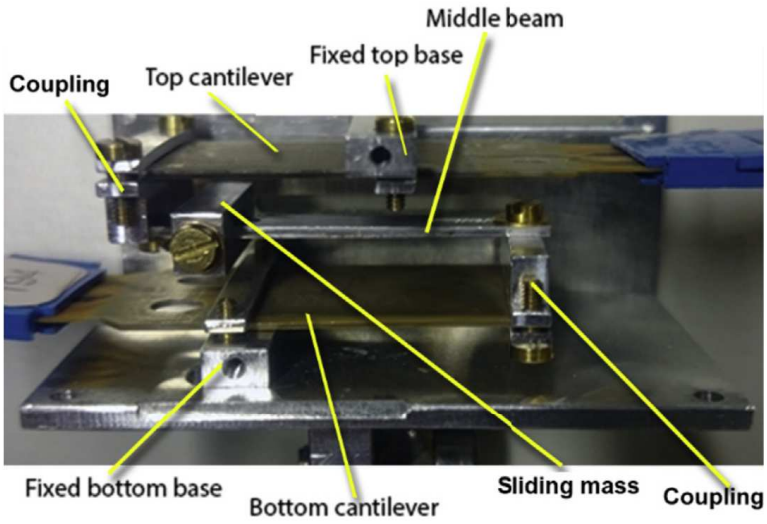

Figure 3.17: 4DOF self-tuning energy harvester seen from the side (one side wall is removed).

3.3.3 Electronics

The use of a power management circuit (MIDE EHE004 [55]) was important for the piezoelectric harvesters in order to convert the AC output into DC output. The EHE004 was combined with a supercapacitor which stored the energy and released power to the transmitter when a certain voltage was reached in the supercapacitor, 4.04 V or 5.05 V depending on the chosen output voltage. When the voltage dropped beneath a certain voltage in the supercapacitor the circuit cut power to the transmitter and the supercapacitor started charging again. The circuit had four different output voltages to choose between (1.8 V, 2.5 V, 3.3 V and 3.6 V), all of them appropriate with the CC2530.

CHAPTER 4

Results

4.1 semiconductor harvester

The semiconductor harvester was never used in a wireless sensor system but did nevertheless produce interesting results and knowledge.

4.1.1 Synthesis results

The synthesis of $Ba_8Ga_{16}Ge_{30}$ resulted in a highly crystalline material (synthesis method explained in **paper I**). This material could, without further processing, be cut into pellets to be used for the module. The measured Seebeck coefficient peaked at 700°C with 185 μV/K, with resistivity at 300 Ω/cm and a thermal conductivity based on previous work [78], this gave a zT-value of 0.83 at 700°C, see Fig. 4.1.

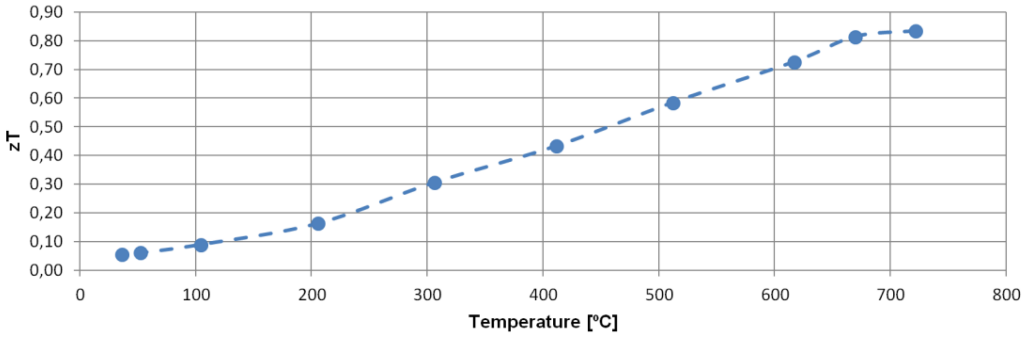

Figure 4.1: Resulting zT-value from $Ba_8Ga_{16}Ge_{30}$ synthesis.

The La-doped $Yb_{14}MnSb_{11}$ was a more problematic material and the resulting crystalline material was covered in tin-flux from the synthesis method (in **paper I**). The tin flux was removed inside an argon filled glove box but the size of the crystals was not big enough (2 mm $\times$ 2 mm $\times$ 8 mm required) for proper thermoelectric measurements. The Seebeck coefficient could however be measured up to 195°C with a Seebeck coefficient reaching 30 μV/K, see Fig. 4.2.

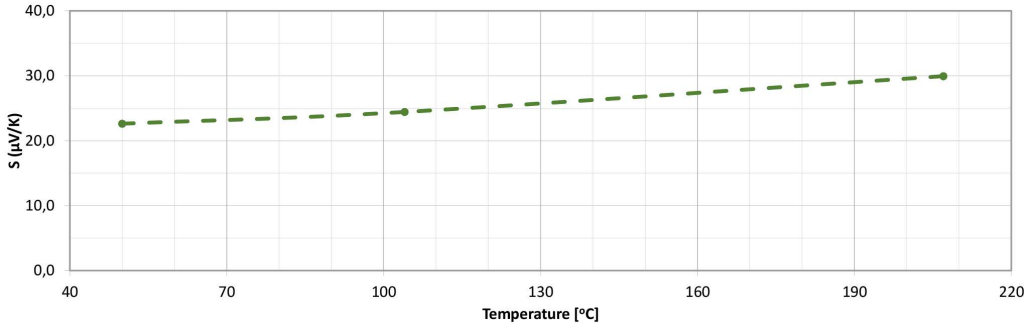

Figure 4.2: Seebeck coefficient measurement from La-doped $Yb_{14}MnSb_{11}$ synthesis.

4.1.2 Harvester measurements

Because of the challenges with the p-type material and the leg size discussed in section 3.1.1 and 3.1.2, the assembled thermoelectric energy harvesters had an area ratio of 1:1 and was comprised of one single thermocouple of La-doped $Yb_{14}MnSb_{11}$ and $Ba_8Ga_{16}Ge_{30}$.

Voltage measurements were conducted during and after the curing of the outermost glue. During the curing procedure the harvester was locked tight between two aluminium blocks, one with active cooling and one acting as heat source. The temperature on the hot side was slowly cooled down from 224°C to 48°C and started with a maximum environmental temperature gradient of 176°C, see Fig. 4.3. The measured voltage from the device reached 18.5 mV, about 70 % of simulated voltage.

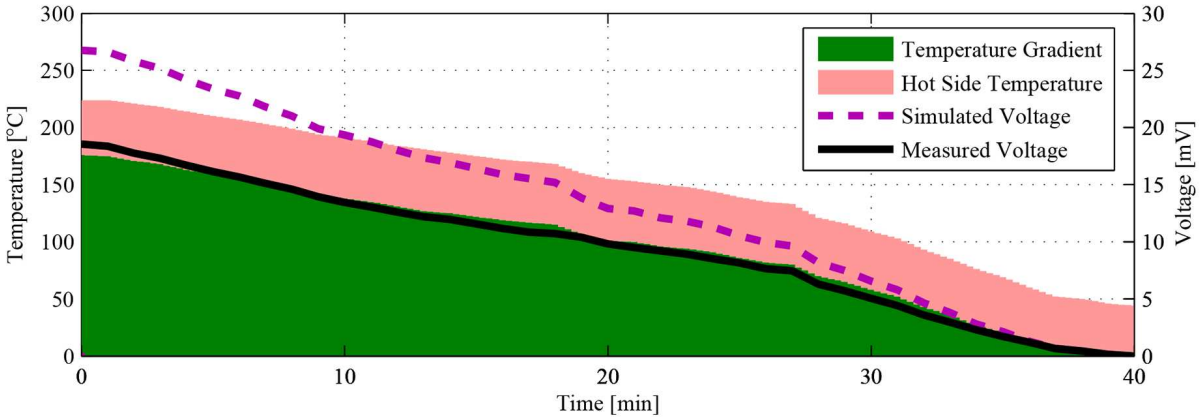

Figure 4.3: Hot side temperature (pink fill) and temperature gradient (green fill). The measured voltage (black solid line) is compared with the simulated voltage (purple dashed line).

Since the harvester (because of known Seebeck coefficients) essentially was a thermocouple temperature sensor and the measured Seebeck values was used in the simulations, the actual temperature gradient inside the harvester was about 70% of the environment. Based on the Seebeck values the temperature gradient inside the module reached approximately 123°C.

For higher temperatures a change of test rig was necessary. The furnace for high temperatures was equipped with an Inco600 rod inserted into the furnace through a hole in the bottom. This rod was used on the cold side of the harvester and the temperature was measured next to the harvester. A copper heat flange was placed on top of the harvester to absorb and distribute heat to the harvester.

The temperature was slowly increased over 150 minutes without active cooling on the Inco600 rod, see Fig. 4.4. The thermal gradient was controlled by controlling the temperature increase. At approximately 280°C air temperature (160°C thermal gradient) something happened inside the harvester which reduced the voltage output. The voltage continued to increase as expected after this reduction until 500°C where it suddenly regained the lost voltage output.

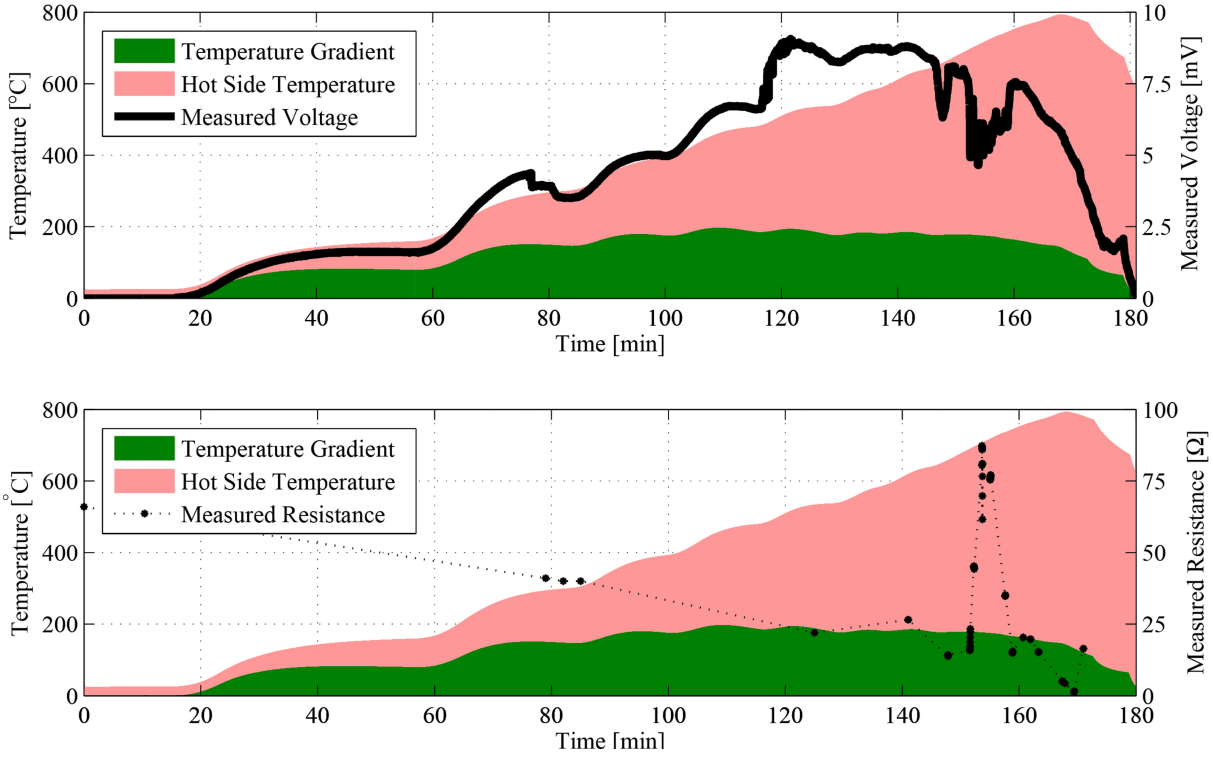

Figure 4.4: Hot side temperature (pink fill) and temperature gradient (green fill) during measurement of harvester voltage (black solid line, top figure) and resistance (points, bottom figure).

From 600°C the furnace was set to full power in an attempt to keep the thermal gradient at 200°C, until 800°C was reached, and the furnace was shut down. The voltage dip and increased resistance at 650-750°C indicates that there is insufficient contact between the thermoelectric materials and the electrodes. This was somewhat visually confirmed by a deforming copper heat flange on top of the harvester.

4.1.3 Sources of error

The Seebeck coefficient measured on the La-doped $Yb_{14}MnSb_{11}$ stopped at 207°C where the thermoelectric rod broke in half. The rod was the only part that was big enough for Seebeck coefficient measurements but suffered from some visible tin inclusions in the middle of the rod. Although the inclusions looked superficial it is possible that the thermoelectric rod broke because the tin melted and big parts were made of tin, leaving a thin rod of La-doped $Yb_{14}MnSb_{11}$ under pressure. If this was the case, then the measured Seebeck coefficient could be too low.

The low temperature measurement reached only about 70% of the simulated value. This means that if the measured Seebeck coefficient of the p-type material was accurate (see above), the thermal gradient over the thermoelectric materials only reached 123°C. The rest of the temperature gradient was lost in the base plates, the electrodes and all the contact interfaces between the environment and the thermoelectric legs. All the measurements were performed without thermal paste that would improve the thermal conductance to the harvester. For the low temperature measurements thermal paste was possible, but with the harvester so unique and precious it could not be risked using thermal paste that potentially could damage the harvester before the measurements at GKN Aerospace.

The reduced voltage output (8.5 mV versus 75 mV in simulations) during the high temperature measurement could indicate a bad contact inside the harvester and/or poor thermal contact with the cooling rod or copper flange. Poor thermal contact seemed likely due to the rough surface on the Inco600 cooling rod. Also, inspection of the copper heat flange after the measurement also showed a rough and bent surface, distorted by the heat. Unfortunately, no resistance measurements were done close before the first voltage drop at 280°C air temperature. During the second voltage drop, measurements on the resistance show a correlation between the resistance and the reduced voltage. A probable dual explanation to the bad contact comes from the copper heat flange, acting as both a thermal transfer unit and a mass to maintain pressure on the thermoelectric legs. With the apparent distortion at higher temperatures the pressure on the legs could be uneven and with poor contact to the electrodes (both thermally and electrically) as a result.

4.2 All-metal harvester

Two designs with different parameters and insulation were investigated and measured both with and without power management electronics.

4.2.1 Harvester measurements

Paper III covers the load resistance measurements of the short harvester between 40°C and 269°C and the load resistance measurements of the long harvester between 31°C and 241°C, see Fig. 4.5.

For both harvesters the load resistance increased, by 0.04 Ω for the 3-couple harvester and

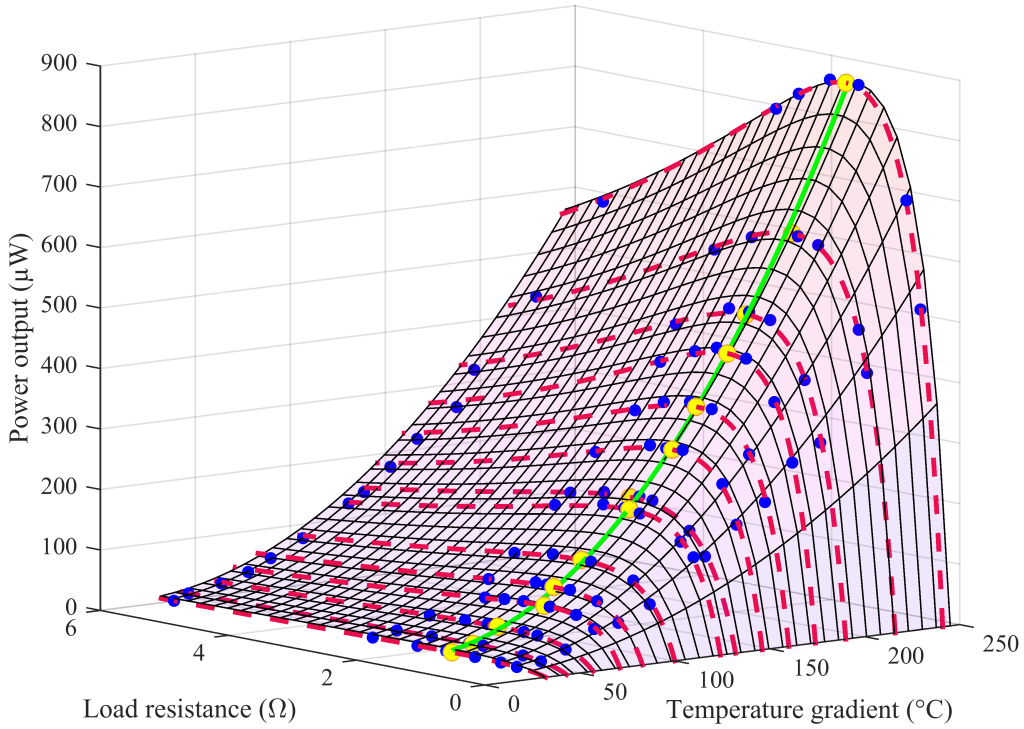

Figure 4.5: Power output at different load resistances (0.35-5.90 Ω) and temperatures. Blue dots are measured values, red dashed lines are curve fitted values. Load resistance match in yellow dots with the green line representing the curve fitted load resistance match from 31-241°C.

0.05 Ω for the 10-couple harvester. This corresponded to an average increased temperature of approximately 100°C for the short harvester, which was considered reasonable.

However, the long harvester had a total resistance increase of 0.05 Ω, only 0.01 Ω more resistance than the 3-couple harvester, but with 7 additional couples and further to the cooling ice bath. The calculated increase in resistance with the measured temperature profile (Fig. 4.6) reached 0.44 Ω.

The discrepancies seen between the measured and calculated load resistance could come from the contact resistance. Adding a temperature dependent contact resistance in the analytical model and fitting the measurements to the model gave an approximation of the contact resistance. The calculated total contact resistance at 241°C was 0.0380 Ω which increased to 0.105 Ω at 31°C. With 2n+1 welds this gave a contact resistance of 1.8 $\mu\Omega$/weld at 241°C and 5 $\mu\Omega$/weld at 31°C. The large difference between cold and hot contact resistance and the high contact resistance of this 1 spot/weld contact, compared to a study by Brand et al. where a resistance spot welder with 4 spots/weld gave 0.2 $\mu\Omega$ [119], indicates that one or more contacts have a poor weld.

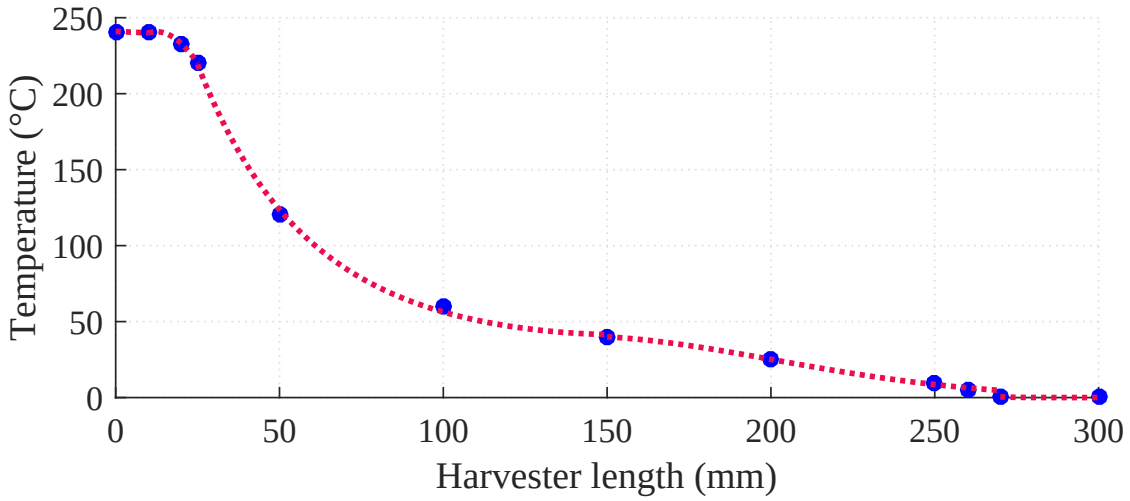

Figure 4.6: Measured temperature (blue dots) along the length of the 300 mm harvester with hot side at 241°C and cold side at 0°C.

4.2.2 Wireless sensor powering

Measurements were conducted with two different wireless transceivers, the CC2530 and ESP8266. These transceivers were modified from their standard versions to reduce power consumption, both by coding and from physical alterations (see **paper III**).

The start-up requirements were the biggest obstacles, with start-up energy consumption of 8.7 mJ and 100 ±(25) mJ for the CC2530 and NODEMCU ESP8266 respectively. To achieve this, the power management circuit stored the harvested energy in a supercapacitor (40 mF) until 3.15 V, when the power was released to the wireless transceivers. This supercapacitor was slightly undersized (115 mJ) for the NODEMCU and oversized for the CC2530 transceiver.

The stored energy was enough to power up the NODEMCU ESP8266, connect to internet and upload temperature data to the cloud. For the less power hungry CC2530 the data was instead sent to a base station for readout.

Charging the capacitor required approximately 6 minutes of harvesting at 241°C temperature gradient. With a smaller capacitor more suitable for the CC2530 it could be fully charged in 30 seconds.

4.2.3 Sources of error

The electric resistance was expected to increase with increased temperature but remained relatively stable. The measured resistance of the harvester at room temperature was also slightly higher than expected. One explanation for this could be the contacts (possibly one poor weld)

and that the contact resistance therefore reduced with increased temperature, from increased stress or pressure from thermal expansion (The 300 mm harvester only fitted one single spot weld).

4.3 Piezoelectric harvesters

4.3.1 Coupled harvester

Paper IV focused on a proof of concept harvester with a backfolded coupled harvester. This coupled harvester did not use metal couplings, to make it more suitable for gas turbine operation.

The simulations predicted resonance peaks at 102.7 Hz and 175.7 Hz and, due to the extended stress distribution, with a power output exceeding two single cantilevers tuned to the same resonance frequencies. However, the measured resonance modes for the prototype were 85.2 and 135.5 Hz with a relative deviation from the simulations of 20.5% and 26.6% respectively. The measured power output was also lower than the simulated power output.

Based on Eq. 2.6 and 2.7 this behaviour points towards lower stiffness and increased damping in the prototype compared to the simulations, with the lower stiffness being the main cause of the lower resonance frequency. This frequency discrepancy occurred despite the use of the same materials in the cantilevers and the same PTFE couplings as the prototype. The model did however not use PTFE screws to hold the couplings together, instead it was flawlessly merged with the cantilevers in the model. In reality, the connection between the cantilever and the coupling were not merged, or even perfectly smooth surfaces, and the PTFE screws used for clamping could not be tightened very hard because of the soft material.

The solution to increase accuracy was to introduce a 10 μm thick layer of soft material (in the simulations) between the coupling and the cantilevers and thus creating a gap that represents the bad coupling connection and the stress in the screws, see Fig. 4.7.

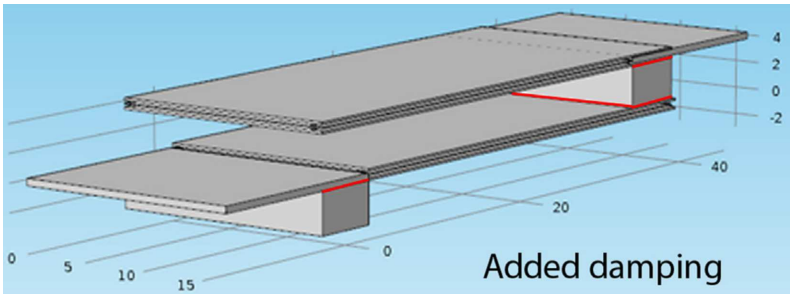

Figure 4.7: The thin damping blocks are marked by red on the model in COMSOL. There are three attenuation zones between the cantilevers and the PTFE pieces.

With the introduced damping the resonance frequencies of the simulated harvester had improved matching with the measured harvester, however with higher power output, see Fig. 4.8.

Additional measurements were conducted to inspect two gas turbine specific properties of the

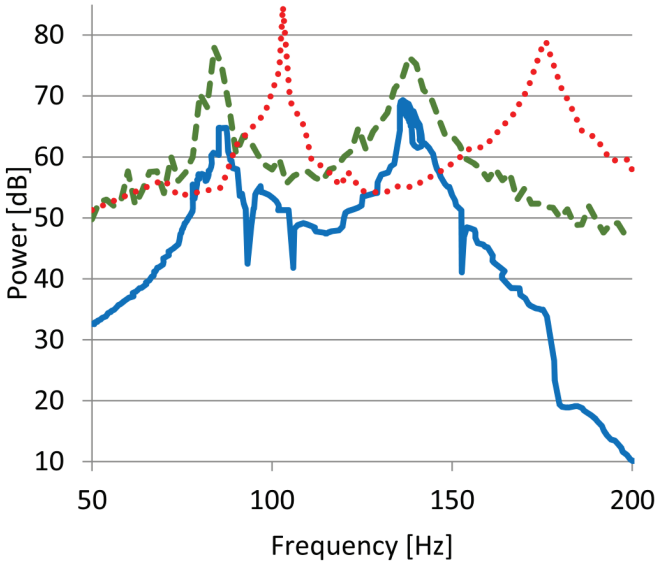

Figure 4.8: Simulated power output of the coupled harvester without damping (red dotted line) and with damping (green dashed line). Measured results in blue.

harvester further, how the harvester will be affected by increased temperature and possible high acceleration vibrations.

The temperature measurements were conducted under moderate vibrations, giving about 8 V voltage output at room temperature from a single cantilever. With increased temperature the resonance frequency and voltage output dropped slightly, reduced by approximately 2 Hz from 150 Hz and approximately 1-2% voltage output at 100°C. This was far below the rated maximum operating temperature of the cantilevers at 150°C [90].

The high acceleration vibration measurements were conducted to examine the durability of the harvester design, all under elevated temperatures of approximately 50-70°C. In this violent series of measurements, the acceleration was slowly ramped up until something broke. Couplings, solder joints and cables were the first to give up and small redesigns with better fasteners for the couplings and plaited high vibration durable cables were introduced. In the final measurement the harvester reached a maximum possible voltage output of 80 V with approximately 3 g sinusoidal RMS acceleration. With increased acceleration, continuing to 10 g sinusoidal RMS acceleration there were some degradation in the harvester and the voltage output slowly decreased from the initial 80 V to 76 V during a 30 min measurement at 10 g.

Paper V continued the work on coupled harvesters with further analysis of different configurations of couplings, tip masses, clamping points and cantilever drill hole patterns. The problematic PTFE couplings in **paper IV** was exchanged with aluminium couplings of various sizes.

Paper V did not rely on COMSOL simulations, instead on experimental measurements backed up by an analytical model. The aim was to see how different configurations affect the resonance peaks, voltage- and power output.

The results from different configurations can be reduced to four main points.

1. When changing the tip mass on the top cantilever, the largest impact was a shift in the peaks, with lower resonance frequencies with larger tip mass.

2. The cantilever drill patterns changed the power output of the top cantilever, but also shifted the resonance peaks (possibly due to different mass).

3. The coupling size mainly affected the power output of the bottom cantilever.

4. The clamping location had the largest impact on the resonance peak separation.

An analytical model was also used to optimize the top cantilever length. The model predicted a reduced peak separation with a minimum at 4 mm top cantilever reduction. Experimental verification was done by cutting the top cantilever length in 2 mm steps and measure the voltage output with minimum peak separation found at 4 mm reduction, see Fig. 4.9.

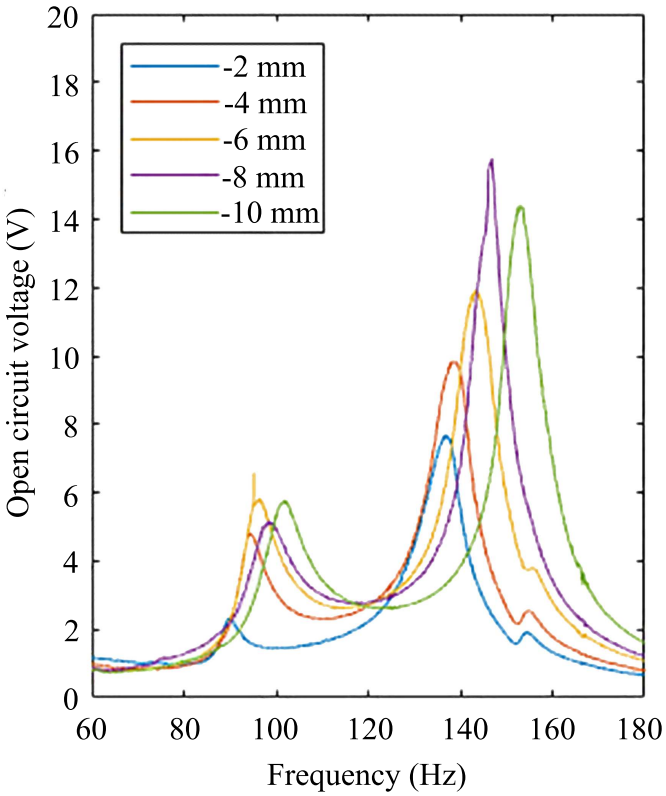

Figure 4.9: Open circuit voltage output for the backfolded harvester with shortened top cantilever from -2 mm to -10 mm.

The optimum configuration would probably be 6 mm, 8 mm or 10 mm shorter top cantilever, depending on application. The peak separation is larger than for -4 mm, but with higher peak voltage output and higher voltage output between the peaks. The voltage requirement for the power management electronics (EHE004) was 3.1 V and would function poorly below that voltage [90]. Higher voltage output between the peaks was therefore an important factor. The -8 mm peak reduction was most suitable for the electronics (highest voltage between the peaks) and therefore chosen for further measurements.

Load resistance measurements were conducted on the -8 mm harvester (see **paper V**). The load

	Load resistance match	Power output
Bottom: Peak 1	30 (±5) kΩ	0.57 mW
Top: Peak 1	60 (±10) kΩ	0.03 mW
Bottom: Peak 2	23 (±2) kΩ	0.76 mW
Top: Peak 2	40 (±5) kΩ	1.20 mW
Both: Peak 1	30 (±2) kΩ	0.60 mW
Both: Peak 2	32 (±3) kΩ	1.85 mW

TABLE 4.1: Load resistance matching for peak 1 (bottom and top) and peak 2 (bottom and top). The required load differs between peaks and cantilever. The optimal load resistance for both cantilevers combined is similar for peak 1 and 2 at 30-32 kΩ.

resistance of the two cantilevers at both peaks were investigated, see Table. 4.1.

The load resistance was purely resistive and gave different load resistance match for both the cantilevers and the resonance peaks, ranging from 23 kΩ to 60 kΩ. A collective load resistance of 30 kΩ gave the best total power output with 1.80 mW.

4.3.2 Self-tuning harvester

Two designs were compared, one with a 25 mm long middle beam (Table 4.2) and one with a 11 mm long middle beam (Table 4.3). The measurements compared the voltage output from a fixed mass on the beam and a sliding mass. The aim of the measurements was to confirm the analytical model, see **paper VI**.

Long beam	Length	Thickness	Width
Beam	25 mm	1 mm	3 mm
Top cantilever	23 mm	0.89 mm	18 mm
Bottom cantilever	21 mm	0.89 mm	18 mm

TABLE 4.2: Length, width and thickness of long middle beam and cantilevers.

Short beam	Length	Thickness	Width
Beam	11 mm	1 mm	3 mm
Top cantilever	14 mm	0.89 mm	18 mm
Bottom cantilever	12 mm	0.89 mm	18 mm

TABLE 4.3: Length, width and thickness of short middle beam and cantilevers.

The measured difference between a sliding and a fixed mass was broader bandwidth. For both the short and the long beam the fixed mass had 8 Hz bandwidth at 3 dB and the sliding mass had 12 Hz bandwidth at 3dB. The peak open circuit voltage increased for the long beam (11.5 V to 11.7 V) and decreased for the short beam (3.26 V to 3.12 V), see Fig. 4.10.

Best efficiency from electronics was achieved if the power electronics was powered with a voltage input above 5.13 V [120]. For the long beam design this was achieved with an effective

bandwidth of 22 Hz.

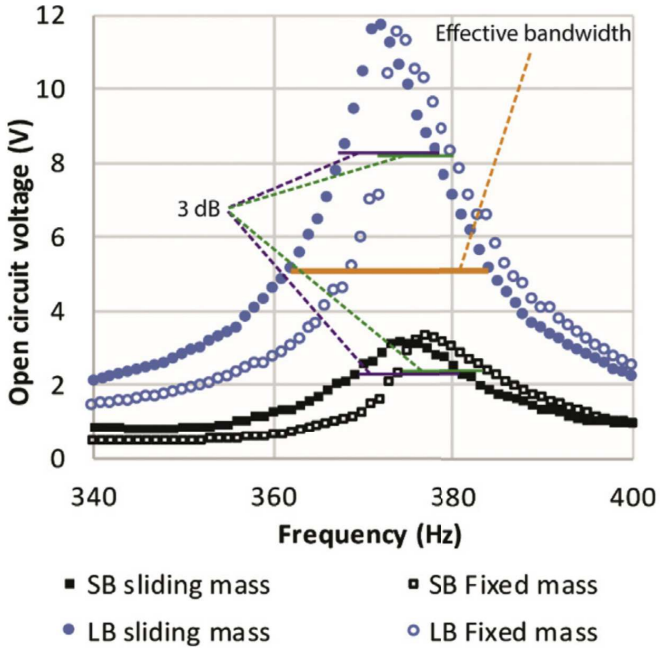

Figure 4.10: Measured open circuit voltage output with fixed mass and sliding mass over 340-400 Hz for the short beam (SB) and the long beam (LB).

When the driving frequency was applied, the mass moved towards either edge of the middle beam (given that it started out in the centre of the beam). The sliding pattern was the same regardless of the direction. In the two tests with asymmetric setup (i.e. long and short beam) with different lengths of the top and bottom piezoelectric cantilevers, the sliding mass moved from the centre to an outer position but also had intermittent sliding behaviour during the frequency sweep where the sliding was unstable. The unstable sliding was clearly visible with the mass moving back and forth (approximately 3 mm along the middle beam at 362-366 Hz), see Fig. 4.11.

4.4 Gas turbine measurements

During the time period when access to the gas turbine was available, no thermoelectric energy harvester was assembled and ready for measurements. A feasibility test was instead done at lower temperatures with a commercial thermoelectric harvester with a size of 40 mm $\times$ 40 mm. The harvester was placed between a copper block and an actively cooled CPU-fan, see Fig. 4.12.

The voltage output from the harvester quickly reached 5 V before the harvester melted during the first run. A voltage output above 1.2 V was enough to start the wireless sensor which made it feasible to power the transceiver without any power management electronics. During the following tests the harvester was thermally insulated from the heat source to keep the thermoelectric

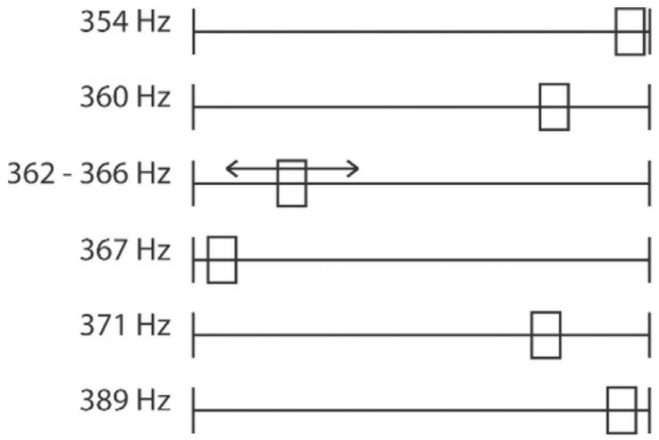

Figure 4.11: The position of the mass on the middle beam is shifting, depending on applied frequency on the system.

module from melting. When the voltage output reached 1.2 V the wireless sensor started up and sent temperature measurements. Because of the active cooling the harvester could sustain the wireless sensor until turbine shut down.

Several trips were made to Rolls-Royce PLC® in Derby, England to measure on an ex-service gas turbine. Even with the data from previous measurements on the engine as well as the vibrational data from Rolls-Royce® measurements it proved too difficult to prepare the coupled harvesters before arrival, despite having several differently tuned coupled harvesters (with PTFE couplings from **paper IV**) at our disposal.

None of the coupled harvesters showed the promising power output seen in the simulations and shaker table measurements and charging the supercapacitor took more than 30 minutes. The power output from the harvester was however enough to charge the supercapacitor, start the ZigBee wireless sensor and send the temperature data to the control room for approximately 75 s, see Fig. 4.13. The start up sequence takes a large part of the available energy in the supercapacitor and is discharged to 2.95 V over the next 75 s with constant transmitting of temperature data. At 2.95 V the power management cuts power and the supercapacitor start to charge again.

Attempts to re-tune the harvesters on site was unsuccessful because of the complexity of tuning them by hand. Because of the easy calibration of a single cantilever an attempt to use 10 single cantilevers did reach slightly higher voltage output than the coupled harvesters but still not enough to power the CC2530 ZigBee transceiver [57] for continuous drive. Based on the power requirement of the CC2530 and the power output from the harvesters, showed that the CC2530 can only transmit data once every 2 s. This was deemed very good, since once every 10 s was estimated enough for the application.

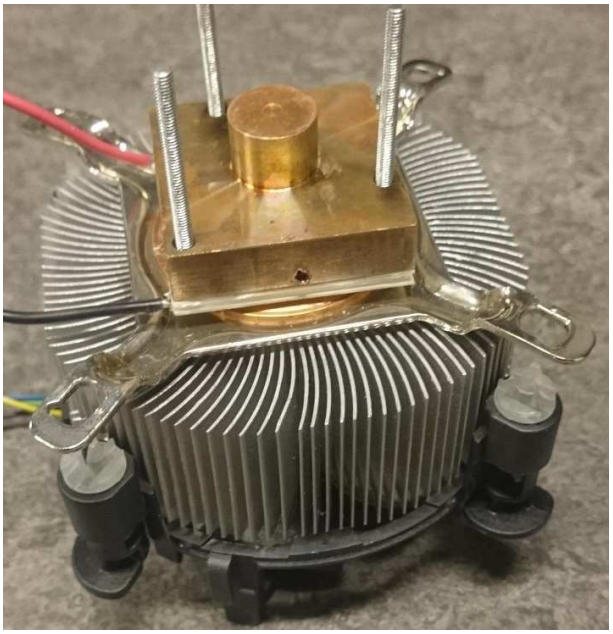

Figure 4.12: A commercial thermoelectric harvester squeezed between a copper block and a CPU block. The copper block was placed on the gas turbine exhaust in an existing mount with the three screws.

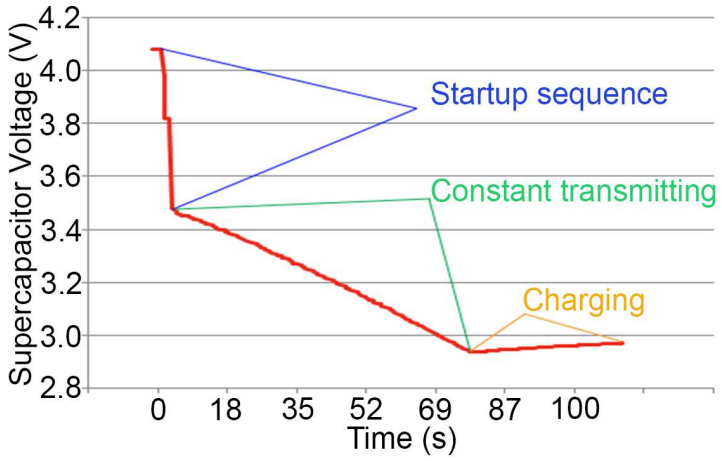

Figure 4.13: Measured supercapacitor voltage during start up and transmission from CC2530 transceiver.

CHAPTER 5

Discussion and conclusion

5.1 Discussion

5.1.1 Thermoelectric harvesters

Semiconductor harvester

Several difficult challenges need to be conquered before the proposed semiconductor harvester could power a wireless sensor in a gas turbine. Without the bonding of electrodes and thermoelectric materials the harvester suffers from high contact resistance, with lower power output as a result. However, even with this part solved the harvester is located where no power electronics can function and high temperature cables are required to reach power management electronics and transceiver.

The commercial thermoelectric harvester used to power the CC2530 sensor node did not require any power management but could not power the sensor node unless 1.2 V was reached. This is a voltage that the semiconductor harvester could never reach with its current design. A 7-couple device with higher voltage output was successfully assembled during the project but this 4-month synthesis and assembly were destroyed in an unfortunate accident during the final stage, when sealing with Renolit 762 glue. All voltage measurements on this device were done inside a glovebox without proper temperature measurements. To keep within the project deadlines the decision was therefore to build 1-couple harvesters with the material still available.

The materials $Ba_8Ga_{16}Ge_{30}$ and La-doped $Yb_{14}MnSb_{11}$ had never been tried before in a harvester and complications was of course inevitable. The results showed that the material combination could be a viable choice in harvesters in this temperature range. However, no long-term measurements were conducted in this work and long term stability could be an issue [121]. The recommendation is to use materials that are more well-studied, like SiGe. This is especially true if fabrication is planned in a clean room, where both $Ba_8Ga_{16}Ge_{30}$ and $Yb_{14}MnSb_{11}$ are likely to be prohibited in most machines.

Metal harvester

The metal harvester was born from the failures and challenges met when designing and building the semiconductor harvester. With the elongated design this harvester could be located both where electronics can operate and in high temperatures. However, still needing power manage-

ment electronics because of the low voltage output.

One of the concerns with using metals with high thermal conductivity as thermoelectric materials was the heat transfer through the harvester. Attempts were made to measure the heat transfer with a tunable heat source. However, the measurement accuracy was too low to make any conclusions and was not included in the paper. A simple calculation (without accounting for air cooling) shows that the total transferred heat in the 10-couples harvester from 241°C to 0°C only reaches 450 ±50 mW. The explanation for the low heat transfer comes from the thin foils in combination with the 300 mm length, comparing with the thin and wide semiconductor thermoelectric harvester reaching 25 W heat transfer.

The thermal contact resistance in a conventional thermoelectric harvester (Environment to base plates, base plates to electrodes and electrodes to thermoelectric materials) reduces the available temperature gradient over the thermoelectric materials with lower power output as a result. The metal harvester presented in this work has thermal contact resistance between each couple with insulating polyimide tape. Adding couples will increase this resistance. The measured voltage output from each measured temperature still follows the temperature and an explanation is the low thermal heat transfer through the harvester combined with the large contact area between each couple to transfer heat between couples.

The greatest strength of the harvester is its simplicity, with no electrodes, no brittle or sensitive materials, and a simple spot weld to fuse the couples together. With a width of 6 mm each weld could fit 4 spot welds with low contact resistance and high reliability as a result. The glass fiber insulation was difficult to implement over distances longer than 10-20 mm and cannot be recommended unless local temperatures exceed 260-400°C, with polyimide limited in temperature to 400°C, 260°C for polyimide tape. The sturdiness of the harvester does however reduce the amount of possible harvester locations and it cannot be placed in a location where it can come loose and damage the engine.

The choice to complement the CC2530 ZigBee development kit with the NodeMCU ESP8266 is that the internet of things is increasingly important and simple, inexpensive and readily available types of DIY wireless solutions need to be investigated. The cost of the harvester materials ($8) and electronics ($6+$3) ends at a total cost of $17.

The effective power output after power management increases from 23 μW to 290 μW, going from 3-couples to 10-couples. Reducing contact resistance with more spot welds (requires at least 6 mm wide foil) and increasing the number of couples to 30 would increase the effective power output to approximately 1 mW. However, already at 10 couples the harvester is less bendable and starts to feel bulky. The thermal contact resistance would increase substantially and could possibly lower the average temperature gradient.

Even though the harvester maybe lacks technological novelty and stands out in its simplicity, the result is a working harvester with a design that does not exist commercially. The scientific contribution of building a functional harvester from simple materials previously deemed unworthy for power conversion should not be underestimated. Hopefully the work will result in more scientific eyes focused on application design instead of only more efficient thermoelectric materials.

5.1.2 Piezoelectric harvesters

It is possible that all piezoelectric harvester designs presented are too big and heavy for use inside the gas turbine, even without metal couplings it could damage the blades if they were to come loose.

The difference between the measurements and the simulations was substantial without the soft layer in the simulations. Adding a soft layer reduced the stiffness and the difference in resonance between the simulation and the measurement but it is not an elegant solution. After publishing **paper IV**, the couplings were improved significantly by replacing the PTFE with small electrically isolated metal screws and aluminium blocks. This moved the measured resonance frequencies closer towards the simulated values, making it easier to tune, but the added mass reduced the available frequency span.

The coupled harvester is quite durable in the current form, capable of withstanding powerful vibrations. Even though there was harvester degradation at 10 g rms vibrations it did not break. These kinds of vibrations will never occur in any engine unless it is catastrophically unbalanced.

Two different designs on the drilled cantilevers were used as top cantilever, with the goal to mimic a trapezoidal shape which has been shown to yield a more even stress distribution. One of the main reasons behind the choice to drill holes instead of using real trapezoid harvesters is the lack of commercial trapezoid cantilevers, with rectangular shaped cantilevers being the industry standard.

The results on the gas turbine did not give the power output predicted by the shaker table or the simulations. There are a few possible explanations for this behaviour. One of the more likely reasons why it performed poorly is the encapsulation box and the mounting of the box to the gas turbine. The mounting was far from optimal and could possibly be a big damping factor of the entire system. The box itself also made an impact on the resonance frequency and depending on how the box was oriented it gave different results despite using similar mounting method. Tuning the harvesters at site proved to be too difficult even with the pre-tuned markers and different settings prepared with simulations.

With the low power output from the coupled energy harvester the wireless sensor node could not be sustained for continuous sending of data and at least 2 s delay between transmission needs to be implemented to sustain the energy in the supercapacitor.

5.2 Conclusion

Four different energy harvester concepts were developed, a semiconductor thermoelectric energy harvester for the temperature span 600-800°C, a metal thermoelectric energy harvester with long reach, a coupled piezoelectric energy harvester with increased bandwidth and a self-tuning piezoelectric harvester.

The semiconductor thermoelectric energy harvester was designed and built using in-house synthesized n-type and p-type materials. These materials had never been used combined in a harvester before. The intended design with 1:2.6 area ratio was abandoned due to lack of material

and replaced with 1:1 area ratio, giving the design 84% of the planned power output. The measurements in low temperature and high temperature gave results below simulated values and no power measurements or gas turbine measurements were conducted with the thermoelectric harvester. However, the design and sealing of the harvester could work in gas turbines.

Two metal thermoelectric energy harvesters were assembled with 3-couples (55 mm length) and 10-couples (300 mm length). The harvesters were connected to power management electronics and two different wireless transceivers. The power output from the 10-couples harvester after power management reached 290 μW (241°C temperature gradient) and could power up and send temperature data to a receiver. This shows that these types of harvesters are a feasible choice for powering wireless sensor nodes, especially in applications like gas turbines where areas of passive and active cooling overlap.

A coupled piezoelectric harvester was developed to increase bandwidth without losing power output. The initial design had PTFE couplings but suffered from high damping. The design was optimized in **paper V** with increased voltage output between the peaks reaching an impressive effective bandwidth of 70 Hz (92-162 Hz) with a minimum voltage of 2.75 V and maximum power output of 1.80 mW at 0.2 g.

The coupled harvester was subjected to violent vibration tests with 10 g RMS for 30 min, with a degradation of the voltage output reaching 5%, but it did not break.

The gas turbine measurements were made with the coupled piezoelectric harvester and a commercial thermoelectric harvester. The piezoelectric harvester was connected to a power management circuit and managed to power the transceiver for 75 s before the commercial supercapacitor was below the voltage limit. Continuous sending could not be sustained with the piezoelectric harvester. The power output from the harvester could though power the transceiver with 2 s delay between transmission, which is still enough for the application.

The commercial thermoelectric energy harvester was more powerful than the piezoelectric harvester and it was possible to start up and send temperature data with the transceiver, even without any power management or energy storage. The commercial harvester could easily power the transceiver, and if combined with an intelligent system for power distribution a single thermoelectric harvester could power tens of wireless sensors nodes.

5.3 Outlook and future work

No power measurements were conducted on the semiconductor thermoelectric energy harvester. Before conducting any power output measurements it is important to solve the contact issue. The connection of the electrodes to the $Yb_{14}MnSb_{11}$ material can be done by diffusion bonding [86], i.e. heating the materials to 1000°C under high pressure for 12 hours. This is a temperature higher than $Ba_8Ga_{16}Ge_{30}$ can handle so the diffusion bonding needs to be done on $Yb_{14}MnSb_{11}$ separately, before assembly of the device. Diffusion bonding between titanium and other metals can be made at much lower temperatures than 1000°C and bonding a thin layer of Ti with the Mo-electrode can be done at low pressures and 700°C [122]. It is however not known if $Ba_8Ga_{16}Ge_{30}$ can be bonded with Ti without problems.

The metal thermoelectric harvester could power a wireless sensor node, but no live tests were conducted on a gas turbine. Live tests could reveal unforeseen problems with the design and should be undertaken. Further development of the harvester with new materials could improve the design significantly and metals with higher Seebeck coefficient, better high temperature stability and lower high temperature resistivity would be interesting to explore further. For gas turbine applications the focus should be on higher temperature stability, which would require an insulating material with high temperature stability.

To investigate the coupled piezoelectric harvester further, a high temperature version should be constructed from high temperature cantilevers (up to 300°C) and measured at different locations on a gas turbine. More advanced electronics should also be tested with the harvester, with MPPT and/or self-tuning properties.

References

[1] D. Moga, D. Petreus, and N. Stroia, "A Low Cost Architecture for Remote Control and Monitoring of Greenhouse Fields," *2012 7th IEEE Conference on Industrial Electronics and Applications (ICIEA)*, pp. 1940–1944, 2012.

[2] CORDIS, "Sensors Towards Advanced Monitoring and Control of Gas Turbine Engines," *CORDIS*, vol. 314061, 2012-2016.

[3] UDI-2, "Utlysning steg 2 - samverkansprojekt," *Vinnova*, 2019.

[4] S. Pay and Y. Baghzouz, "Effectiveness of Battery-Supercapacitor Combination in Electric Vehicles," *IEEE Bologna Power Tech Converence*, vol. 23-26 July, 2003.

[5] Rolls-Royce, "The Jet Engine," *Rolls Royce Technical Publications; 5th ed. edition*, 1996.

[6] A. Cuadrasa, M. gasulla, and V. Ferrari, "Thermal energy harvesting through pyroelectricity," *Sensors and Actuators A*, vol. 158, pp. 132–139, 2010.

[7] J. Ericsson, "The caloric engine," *Journal of the Franklin Institute*, vol. 18, pp. 48–53, 1834.

[8] S. Carnot, "Rflexions sur la puissance motrice du feu et sur les machines propres dvelopper cette puissance," *Paris: Bachelier*, vol. 55, 1824.

[9] J. M. Gordon and M. Huleihil, "General performance characteristics of real heat engines," *Journal of Applied Physics*, vol. 72, p. 829, 1992.

[10] P. Chiesa and E. Macchi, "A Thermodynamic Analysis of Different Options to Break 60% Electric Efficiency in Combined Cycle Power Plants," *J. Eng. Gas Turbines Power*, vol. 126(4), pp. 770–785, 2004.

[11] C. B. Vining, "An inconvenient truth about thermoelectrics," *Nature materials*, vol. 8, pp. 83–85, 2009.

[12] F. Liu, A. Phipps, S. Horowitz, K. Ngo, L. Cattafesta, T. Nishida, and M. Sheplak, "Acoustic energy harvesting using an electromechanical Helmholtz resonator," *The Journal of the Acoustical Society of America*, vol. 123, pp. 1983–1990, 2008.

[13] L. Dhakar, "Triboelectric Devices for Power Generation and Self-Powered Sensing Applications," *Springer; 1st ed. 2017 edition*, 2017.

[14] Y. Chiu and V. F. G. Tseng, "A capacitive vibration-to-electricity energy converter with integrated mechanical switches," *J. Micromech. Microeng.*, vol. 18, pp. 104 004, 1–8, 2008.

[15] J. Huang, R. O'Handley, and D. Bono, "High efficiency vibration energy harvester," Jan. 10 2006, uS Patent 6,984,902. [Online]. Available: https://www.google.com/patents/US6984902

[16] S. P. Beeby, M. J. Tudor, and N. M. White, "Energy harvesting vibration sources for microsystems applications," *Meas. Sci. Technol.*, vol. 17, pp. R175–R195, 2006.

[17] T. Krupenkin and J. A. Taylor, "Reverse electrowetting as a new approach to high-power energy harvesting," *Nature Communications*, vol. 2, p. 448, 2011.

[18] S. Roundy and P. K. Wright, "A piezoelectric vibration based generator for wireless electronics," *Smart Mater. Struct.*, vol. 13, p. 11311142, 2004.

[19] S. Boisseau, G. Despesse, and B. A. Seddik, "Electrostatic Conversion for Vibration Energy Harvesting, Small-Scale Energy Harvesting," *InTech*, 2012. [Online]. Available: https://www.intechopen.com/books/small-scale-energy-harvesting/electrostatic-conversion-for-vibration-energy-harvesting

[20] J.-H. Yoo, A. Flatau, and A. Purekar, "Performance of galfenol energy harvester at high temperature," *ASME 2011 Conference on Smart Materials, Adaptive Structures and Intelligent Systems, SMASIS 2011*, vol. 1, 01 2011.

[21] J. Wu, H. Shi, T. Zhao, Y. Yu, and S. Dong, "High-temperature $BiScO_3$-$PbTiO_3$ piezoelectric vibration energy harvester," *Advanced Functional Materials*, vol. 26, no. 39, pp. 7186–7194, 2016. [Online]. Available: http://dx.doi.org/10.1002/adfm.201602645

[22] S. Barker, K. V. Vassilevski, N. G. Wright, and A. B. Horsfall, "High temperature vibration energy harvester system," in *2010 IEEE Sensors*, Nov 2010, pp. 300–303.

[23] Z. Chen, Y. Yang, and G. Deng, "Analytical and experimental study on vibration energy harvesting behaviors of piezoelectric cantilevers with different geometries," *1st International Conference on Sustainable Power Generation and Supply, SUPERGEN 09*, pp. 1–6, 2009.

[24] V. Ramadoss, H. Alam, and R. Seeram, "Profile geometric effect of cantilever piezoelectric device using flexural mechanism," *IJNTR*, vol. 4(9), pp. 39–42, 2018.

[25] C. Wei and X. Jing, "A comprehensive review on vibration energy harvesting: modelling and realization," *Renew. Sustain. Energy Rev.*, vol. 74, pp. 1–18, 2017.

[26] P. Li, F. Jin, and J. Yang, "A piezoelectric energy harvester with increased bandwidth based on beam flexural vibrations in perpendicular directions," *IEEE Trans. Ultrason. Ferroelectr. Frequency Control*, vol. 60(10), pp. 2214–2218, 2013.

[27] U. Wagner and P. Hagerdorn, "Piezo-beam systems subjected to weak electric field: experiments and modelling of non-linearities," *J. Sound Vib.*, vol. 256(5), pp. 861–872, 2002.

[28] G. Gafforelli, A. Corigliano, R. Xu, and S.-G. Kim, "Experimental verification of a bridge-shaped, nonlinear vibration energy harvester," *Appl. Phys. Lett.*, vol. 105, p. 203901, 2014.

[29] L. Gu and C. Livermore, "Impact-driven, frequency up-converting coupled vibration energy harvesting device for low frequency operation," *Smart Mater. Struct.*, vol. 20, pp. 1–10, 2011.

[30] X. Zhao, Z. Shang, G. Luo, and L. Deng, "A vibration energy harvester using AlN piezoelectric cantilever array," *Microelectron. Eng.*, vol. 142, pp. 47–51, 2015.

[31] G. Sebald, H. Kuwano, D. Guyomar, and B. Ducharne, "Experimental duffing oscillator for broadband piezoelectricenergy harvesting," *Smart Mater. Struct.*, vol. 20(10), p. 102001, 2011.

[32] H. Xiao, X. Wang, and S. John, "A dimensionless analysis of a 2dof piezoelectric vibration energy harvester," *Mech. Syst. Signal Process.*, vol. 58, pp. 355–375, 2015.

[33] H. Wang, L. Tang, Y. Guo, X. Shan, and T. Xie, "A 2DOF hybrid energy harvester based on combined piezoelectric and electromagnetic conversion mechanisms," *J. Zhejiang Univ. Sci. A*, vol. 15(9), pp. 711–722, 2014.

[34] S.-J. Jang, E. Rustighi, M. Brennan, Y. Lee, and H.-J. Jung, "Design of a 2dof vibrational energy harvesting device," *J. Intell. Mater. Syst. Struct.*, vol. 22(5), pp. 443–448, 2011.

[35] N. Sharpes, A. Abdelkefi, H. Abdelmoula, P. Kumar, J. Adler, and S. Priya, "Mode shape combination in a two-dimensional vibration energy harvester through mass loading structural modification," *Appl. Phys. Lett.*, vol. 109(3), p. 033901, 2016.

[36] J. Kluger, T. Sapsis, and A. Slocum, "Robust energy harvesting from walking vibrations by means of nonlinear cantilever beams," *J. Sound Vib.*, vol. 341, pp. 174–194, 2015.

[37] X. Tang and L. Zuo, "Enhanced vibration energy harvesting using dual-mass systems," *J. Sound Vib.*, vol. 330(21), pp. 5199–5209, 2011.

[38] I. Kim, H. Jung, B. Lee, and S. Jang, "Broadband energy-harvesting using a two degree-of-freedom vibrating body," *Appl. Phys. Lett.*, vol. 98(21), p. 214102, 2011.

[39] A. Harb, "Energy harvesting: State-of-the-art," *Renew. Energy*, vol. 36(10), pp. 2641–2654, 2011.

[40] H. Wu, L. Tang, Y. Yang, and C. Soh, "A novel two-degrees-of-freedom piezoelectric energy harvester," *J. Intell. Mater. Syst. Struct.*, vol. 24(3), pp. 357–368, 2013.

[41] M. Lallart, S. R. Anton, and D. J. Inman, "Frequency self-tuning scheme for broadband vibration energy harvesting," *Journal of Intelligent Material Systems and Structures*, vol. 21(9), pp. 897–906, 2010.

[42] D. Guyomar and M. Lallart, "recent progress in piezoelectric conversion and energy harvesting using nonlinear electronic interfaces and issues in small scale implementation." *Micromachines*, vol. 2(2), pp. 274–294, 2011.

[43] E. S. Leland and P. K. Wright, "Resonance tuning of piezoelectric vibration energy scavenging generators using compressive axial preload," *Smart Mater. Struct.*, vol. 15, p. 1413, 2016.

[44] J. F. Gieras, J.-H. Oh, M. Huzmezan, and H. S. Sane, "Electromechanical energy harvesting system," *United States patent:*, vol. US8222775B2, 2011.

[45] C. Eichhorn, R. Tchagsim, N. Wilhelm, and P. Woias, "A smart and self-sufficient frequency tunable vibration energy harvester," *Journal of Micromechanics and Microengineering*, vol. 21(10), 2011.

[46] L. Miller, P. Pillatsch, E. Halvorsen, P. Wright, E. Yeatman, and A. Holmes, "Experimental passive self-tuning behavior of a beam resonator with sliding proof mass," *J. Sound Vib.*, vol. 332(26), pp. 7142–7152, 2013.

[47] A. Boudaoud, Y. Couder, and M. B. Amar, "A self-adaptative oscillator," *Eur. Phys. J. B*, vol. 9(1), pp. 159–165, 1999.

[48] I. Kozinsky, "Study of passive self-tuning resonator for broadband power harvesting," *PowerMEMS*, pp. 388–391, 2009.

[49] P. Pillatsch, L. Miller, E. Halvorsen, P. Wright, E. Yeatman, and A. Holmes, "Self-tuning behavior of a clamped-clamped beam with sliding proof mass for broadband energy harvesting," *J. Phys. Conf. Ser.*, vol. 476, p. 12068, 2013.

[50] D. L. Huff, "Noise Reduction Technologies for Turbofan Engines," *35th International Congress and Exposition on Noise Control Engineering (INTERNOISE 2006)*, 2007.

[51] P. Woias, M. Islam, S. Heller, and R. Roth, "A low-voltage boost converter using a forward converter with integrated Meissner oscillator," *J Phys Conf Ser.*, vol. 476, p. 012081, 2013.

[52] P. H. Chen, K. Ishida, K. Ikeuchi, X. Zhang, K. Honda, Y. Okuma, Y. Ryu, M. Takamiya, and T. Sakurai, "Startup Techniques for 95 mV Step-Up Converter by Capacitor Pass-On Scheme and VTH-Tuned Oscillator With Fixed Charge Programming," *J Solid-St Circ.*, vol. 47(5), pp. 1252–1260, 2012.

[53] A. Camarda, A. Romani, E. Macrelli, and M. Tartagni, "A 32 mV/69 mV input voltage booster based on a piezoelectric transformer for energy harvesting applications," *Sensor Actuat. A-phys.*, vol. 232, pp. 341–352, 2015.

[54] Datasheet, "LTC3108, Ultralow Voltage Step-Up Converter and Power Manager," *Linear Technology Corporation*, 2010.

[55] MIDE, "EHE004: Energy harvesting electronics," *Data Sheet, rev 2*, 2013.

[56] X.-D. Do, S.-K. Han, and S.-G. Lee, "Optimization of Piezoelectric Energy Harvesting Systems by Using a MPPT Method," *2014 IEEE Fifth International Conference on Communications and Electronics (ICCE)*, vol. 1, pp. 309–312, 2014.

[57] CC2530, "A True System-on-Chip solution for 2.4 GHz IEEE 802.15.4 / ZigBee," *Texas Instruments: Data sheet*, 2014.

[58] A. A. Dahoud and M. Fezari, "NodeMCU V3 For Fast IoT Application Development," *Faculty of IT, Al-Zaytoonah University Amman*, vol. 10, 2018.

[59] X. Luo, J. Wang, M. Dooner, and J. Clarke, "Overview of current development in electrical energy storage technologies and the application potential in power system operation," *Applied Energy*, vol. 137, pp. 511–536, 2015.

[60] M. Haque, Q. Li, A. D. Smith, V. Kuzmenko, E. Köhler, P. Lundgren, and P. Enoksson, "Thermal influence on the electrochemical behavior of a supercapacitor containing an ionic liquid electrolyte," *Electrochimica Acta*, 2018. [Online]. Available: http://www.sciencedirect.com/science/article/pii/S0013468618300434

[61] R. Vullers, R. Von Schaijk, C. Van Doms, and R. Mertens, "Micropower Energy Harvesting," *Solid-State Electronics*, vol. 53, pp. 684–693, 2009.

[62] TECTEG, "MFR," *TECTEG*, 2013. [Online]. Available: http://thermoelectric-generator.com/teg-cascade-800c-hot-side-thermoelectric-power-modules/

[63] G. L. Bennett, "Space Nuclear Power: Opening the Final Frontier," *4th IECEC*, vol. 26-29 June 2006, pp. AIAA 2006–4191, 2006.

[64] N. S. Hudak and G. G. Amatucci, "Small-scale energy harvesting through thermoelectric, vibration, and radiofrequency power conversion," *J. Appl. Phys*, vol. 103, pp. 101 301–1–24, 2008.

[65] TEGpower, "http://www.tegpower.com/index.html," -, vol. -, p. 4 july 2013, 2013.

[66] C. Wan, R. Tian, A. Binti Azizi, Y. Huang, Q. Wei, R. Sasai, S. Wasusate, T. Ishida, and K. Koumoto, "Flexible thermoelectric foil for wearable energy harvesting," *Nano Energy*, vol. 09, 2016.

[67] R. O. Osborn, "Thin, flexible thermoelectric device," *US patent*, vol. US3554815A, 1964.

[68] Z. Lu, M. Layani, X. Zhao, L. P. Tan, T. Sun, S. Fan, Q. Yan, S. Magdassi, and H. H. Hng, "Fabrication of Flexible Thermoelectric Thin Film Devices by Inkjet Printing," *Small*, vol. 10(17), 2014.

[69] T. Zhang, K. Li, J. Zhang, M. Chen, Z. Wang, S. Ma, N. Zhang, and L. Wei, "High-performance,flexible, and ultralong crystalline thermoelectricfibers," *Nano Energy*, vol. 41, pp. 35–42, 2017.

[70] T. J. Seebeck, "Magnetische Polarisation der Metalle und Erze durch Temperatur-Differenz," *Abhandlungen der Königlichen Akademie der Wissenschaften zu Berlin*, vol. 265, 1822-1823.

[71] L. Baranowski, J. Snyder, and E. Toberer, "Concentrated solar thermoelectric generators," *Energy Environ. Sci.*, vol. 5, 9055, 2012.

[72] CAP-xx, "Energy Storage Technologies," *cap-xx*, 2018. [Online]. Available: https://www.cap-xx.com/resource/energy-storage-technologies/

[73] V. Parsonnet, J. Driller, D. Cook, and S. A. Rizvi, "Thirty-One Years of Clinical Experiencewith Nuclear-Powered Pacemakers," *Pace*, vol. 29, pp. 195–200, 2006.

[74] T. M. Tritt, "Thermoelectric Materials: Principles, Structure, Properties, and Applications," *Encyclopedia of Materials: Science and Technology*, vol. 2, pp. 1–11, 2002.

[75] J. Snyder and E. Toberer, "Complex thermoelectric materials," *Nature Materials*, vol. 7, pp. 105–114, 2008.

[76] B. Sherman, R. R. Heikes, and R. W. Ure, "Calculation of Efficiency of Thermoelectric Devices," *American Institute of Physics*, vol. 31, no. 1, 1960.

[77] W. Liu, H. S. Kim, Q. Jie, and Z. Ren, "Importance of high power factor in thermoelectric materials for power generation application: A perspective," *Scripta Materialia*, vol. 111, pp. 3–9, 2016.

[78] A. Palmqvist and et al., "Large thermoelectric figure of merit at high temperature in Czochralski-grown clathrate $Ba_8Ga_{16}Ge_{30}$," *Journal of Applied Physics*, vol. 99, 023708, 2006.

[79] E. Toberer, S. Brown, S. Kauzlarich, and J. Snyder, "High thermoelectric efficiency in lanthanum doped $Yb_{14}MnSb_{11}$," *Applied Physics Letter*, vol. 93, 062110, 2008.

[80] Z. Tian, S. Lee, and G. Chen, "A Comprehensive Review of Heat Transfer in Thermoelectric Materials and Devices," *Annu. Rev. Heat Transf.*, vol. 17, pp. 425–483, 2014.

[81] D. Snyder, J. Himes, and M. Pravda, "Direct heat injection path radioisotopic thermoelectric generator," *US Patent: US3833428A*, 1969.

[82] T. R. Barker, W. L. Kershaw, G. S. Stivers, and J. L. Thomas, "Radioisotope Thermoelectric Generator," *US Patent: US3615869*, 1971.

[83] M. Duff and J. Towey, "Two Ways to Measure Temperature Using Thermocouples Feature Simplicity, Accuracy, and Flexibility," *Analog Dialogue*, vol. 44-10, 2010.

[84] N. R. Muktinutalapati, "Materials for Gas Turbines An Overview," *InTech*, 2011.

[85] J. Paik, E. Brandon, T. Caillat, P. Ewell, and J. Fleurial, "Life testing of $Yb_{14}MnSb_{11}$ for high performance thermoelectric couples," *Proceedings of Nuclear and Emerging Technologies for Space*, vol. (2011), 2011.

[86] S. Firdosy, B. C.-Y. Li, V. Ravi, J. Sakamoto, T. Caillat, R. C. Ewell, and E. J. Brandon, "Metallization for Yb14MnSb11-Based Thermoelectric Materials," *NASA Tech Briefs*, vol. Aug, p. 13, 2011.

[87] E. Wiberg, N. Wiberg, and A. Holleman, "Inorganic Chemistry," *Academic Press*, 2001.

[88] J. Paik and T. Caillat, "Alumina paste layer as a sublimation suppression barrier for $Yb_{14}MnSb_{11}$," *NASA Tech Briefs*, vol. aug, pp. 22–23, 2010.

[89] J.-A. Paik and T. Caillat, "Alumina paste sublimation suppression barrier for thermoelectric device," *United states patent*, vol. US 2010/0229910 A1, p. Sep. 16 2010, 2010.

[90] MIDE, "MIDE: Piezoelectric energy harvesters," *Datasheet*, 2013. [Online]. Available: http://www.tande.com.tw/eh-energy-harvesting/Volture_Datasheet_001.pdf

[91] J. Curie and P. Curie, "Phénomènes électriques des cristaux hémièdres à faces inclinées," *J. Phys. Theor. Appl.*, vol. 1, pp. 245–251, 1882.

[92] P. Dineva, D. Gross, R. Mller, and T. Rangelov, "Dynamic Fracture of Piezoelectric Materials: Solution of Time-Harmonic Problems via BIEM," *Springer Science & Business Media*, 2014.

[93] J. Valasek, "Piezoelectric and allied phenomena in Rochelle salt," *Phys Rev*, vol. 15, p. 537, 1920.

[94] J. W. Waanders, "Piezoelectric Ceramics: Properties & Applications Chapter 2: Physical Basis," *Chapter 2*, 1991.

[95] T. Manzaneque, J. Hernando-Garca, A. Ababneh, P. Schwarz, H. Seidel, U. Schmid, and J. L. Snchez-Rojas, "Quality-factor amplification in piezoelectric mems resonators applying an all-electrical feedback loop," *Journal of Micromechanics and Microengineering*, vol. 21, no. 2, p. 025007, 2011. [Online]. Available: http://stacks.iop.org/0960-1317/21/i=2/a=025007

[96] A. G. Piersol and T. L. Paez, "Harris' Shock and Vibration Handbook: Sixth Edition," *McGraw-Hill*, vol. Ralph E. Blake, Chapter 2: Basic Vibration Theory, pp. 2.18–2.19, 2010.

[97] Gracey, "Piezoelectric Accelerometers Theory and Application," *Metra Mess- und Frequenztechnik*, 2001.

[98] C. Wang, "Timoshenko beam-bending solutions in terms of Euler-Bernoulli solutions," *J. Eng. Mech.*, vol. 121, pp. 763–765, 1995.

[99] P. Auerkari, "Mechanical and physical properties of engineering alumina ceramics," *Espoo: Research notes 1792*, 1996.

[100] M. Ltd, "Mineral Insulated Stainless Steel & Alloy Sheathed Thermocouples & Transducer Cables & Probes," *www.miccltd.com*, vol. Aug, 2017.

[101] D. M. Rowe, "Thermoelectrics Handbook," , *Macro to Nano*, vol. Chapter 11, pp. 1–15, 2005.

[102] S. Song, S. Lee, and V. Au, "Closed-Form Equation for with Variable Thermal Constriction/Spreading Resistance Boundary Condition," *1994 IEPS CONFERENCE*, pp. 111–121, 1994.

[103] S. Lee, "Optimum Design and Selection of Heat Sinks," *Eleventh IEEE SEMI-THERMN Symposium*, 1995.

[104] A. Saramat, E. Toberer, A. May, and J. Snyder, "Thermal stability and phase purity in polycrystalline $Ba_8Ga_xGe_{46-x}$," *Journal of Electronic Materials*, vol. vol 38, No. 7, pp. 1423–1426, 2009.

[105] N. L. Okamoto, T. Nakano, K. Tanaka, and H. Inui, "Mechanical and thermal properties of single crystals of the type-I clathrate compounds Ba8Ga16Ge30 and Sr8Ga16Ge30," *Journal of Applied Physics*, vol. 104, pp. 013 529–1–7, 2008.

[106] V. Ravi, S. Firdosy, T. Caillat, E. Brandon, K. Van Der Walde, L. Maricic, and A. Sayir, "Thermal expansion studies of selected high-temperature thermoelectric materials," *Journal of Electronic Materials*, vol. 38, no 7, pp. 1433–1442, 2009.

[107] V. Ravi, S. Firdosy, T. Caillat, E. Brandon, K. V. D. Walde, L. Maricic, and A. Sayir, "Thermal Expansion Studies of Selected High Temperature Thermoelectric Materials," *JPL Technical Report Server*, vol. 45331, 2014.

[108] Datasheet, "Thermeez 7020 Ceramic Putty," *Cotronics Corporation*, 2001.

[109] P. K. Panda, T. S. Kannan, J. Dubois, C. Olagnon, and G. Fantozzi, "Thermal shock and thermal fatigue study of alumina," *Journal of the European Ceramic Society*, vol. 22(13), pp. 2187–2196, 2002.

[110] I. Tronstad and E. A. Blekkan, "A Study of the Effect of Copper and Additives in Hydrocarbon and Ester Based Insulating Liquids with Isothermal Microcalorimetry," *IEEE Transactions on Dielectrics and Electrical Insulation*, vol. 21(3), pp. 1079–1088, 2014.

[111] Fuchs, "Renolit 762 High Temperature Jointing Compound," *Fuchs*, vol. November, 2008.

[112] Steffca, "Thermic 1100," *Steffca*, 2010.

[113] E. S. Jones, J. F. Mosher, R. Speiser, and J. W. Spretnak, "The Oxidation of Molybdenum," *Corrosion*, vol. 14, pp. 20–26, 1957.

[114] K. Sun, M. A. Stroscio, and M. Dutta, "Graphite c-axis thermal conductivity," *Superlattices and Microstructures*, vol. 45, no. 2, pp. 60 – 64, 2009. [Online]. Available: http://www.sciencedirect.com/science/article/pii/S0749603608002644

[115] C. K. Gupta, "Extractive Metallurgy of Molybdenum," *CRC Press*, pp. 6–8, 1992.

[116] E. Systems, "ESP8266EX Datasheet," *www.espressif.com*, 2018.

[117] J. Brusey, J. Kemp, E. Gaura, R. Wilkins, and M. Allen, "Energy Profiling in Practical Sensor Networks: Identifying Hidden Consumers," *IEEE Sens J.*, vol. 16(15), pp. 6072–6080, 2016.

[118] COMSOL, "COMSOL Multiphysics Reference Manual," *version 5.3*, 2017. [Online]. Available: www.comsol.com

[119] M. J. Brand, P. A. Schmidt, M. F. Zaeh, and A. Jossen, "Welding techniques for battery cells and resulting electrical contact resistances," *Journal of Energy Storage*, vol. 1, pp. 7–14, 2015.

[120] L. Staaf, E. Köhler, J. Kemp, M. Allen, S. Zenkic, A. Lindblom, M. Christodoulou, J. Roberts, P. Lundgren, and P. Enoksson, "Piezoelectric energy harvesting as energy source for autonomous intelligent wireless systems on gas turbines," *EVI-GTI and PIWG Joint Conference on Gas Turbine Instrumentation*, vol. 4(17), 2016.

[121] H. Reardon, A. B. Blichfeld, H. Kasai, H. Yin, E. D. Bøjesen, and B. B. Iversen, "Revealing the slow decomposition kinetics of type-I clathrate Ba8Ga16Ge30," *US Patent: US3615869*, 1971.

[122] J. Sakamoto, A. Kisor, T. Caillat, L. Lara, V. Ravi, S. Fridosy, and J.-P. Fleuiral, "Mo/Ti Diffusion Bonding for Making Thermoelectric Devices," *NASA Tech Briefs*, vol. July 2007, p. 13, 2007.

References